Manuscript Information

Type: General paper

Title: Destructuration of saturated natural loess: From experiments to constitutive modelling

Authors: Yukai Fu[1,2], Zhiwei Gao[3]*, Yi Hong[4], Tonglu Li[1,2], Akhil Garg[5]
*Corresponding author

Information of authors:

Yukai Fu
[1] Department of Geological Engineering, Chang'an University, Xi'an 710054, Shaanxi, China.
[2] Water Cycle and Geological Environment Observation and Research Station for the Chinese Loess Plateau, Zhengning, Gansu, China.
Email: fw@chd.edu.cn.

Zhiwei Gao*
*Corresponding author.
[3] James Watt School of Engineering, University of Glasgow, Glasgow, G12 8QQ, UK. Email: Zhiwei.gao@glasgow.ac.uk.
Tel: +44 141 3303927.

Yi Hong
[4] Key Laboratory of Offshore Geotechnics and Material of Zhejiang Province, College of Civil Engineering and Architecture, Zhejiang University, Hangzhou, Zhejiang 310058, P.R. China. Email: yi_hong@zju.edu.cn.

Tonglu Li
[1] Department of Geological Engineering, Chang'an University, Xi'an 710054, Shaanxi, China.
[2] Water Cycle and Geological Environment Observation and Research Station for the Chinese Loess Plateau, Zhengning, Gansu, China.
Email: dcdgx08@chd.edu.cn.

Akhil Garg
[5] Division of Computational Mathematics and Engineering, Institute for Computational Science, Ton Duc Thang University, Ho Chi Minh City, Vietnam
Faculty of Civil Engineering, Ton Duc Thang University, Ho Chi Minh City, Vietnam
Email: agarg@tdtu.edu.vn.

Abstract

It has been well recognized that unsaturated natural loess shows significant volume contraction upon wetting due to its metastable internal structure. But the structural effect on stress-strain relationship of saturated natural (undisturbed) loess is much less explored. Few attempts have been made in proposing a constitutive model for saturated natural loess. This study presents both laboratory tests and constitutive modelling of a saturated natural loess, with special focus on the structural effect and evolution of structure damage during loading. Oedometer and drained triaxial compression tests have been carried out on undisturbed and remolded saturated loess samples. It is found that the natural soil structure has dramatic influence on mechanical behavior of loess, including the compressibility, dilatancy and shear strength. Destructuration, which is the damage of soil structure with deformation, is observed in both oedometer and triaxial tests. A constitutive model is proposed for saturated loess based on the experimental observations. The model is established within the theoretical framework of subloading and superloading surface concepts. Destructuration of loess is assumed to be affected by both plastic volumetric and shear strain. A new method for determining the initial degree of structure is proposed. The model can reasonably predict the compression and shear behavior of both undisturbed and remolded saturated loess.

Keywords: Destructuration, saturated clayey loess, critical state, constitutive model, drained triaxial compression tests

1. Introduction

Loess, a typical structured soil, is widely distributed in Northwest China. The natural loess was often formed with open and potentially metastable structure due to the arid and semi-arid depositional environment. Such internal structure has significant influence on mechanical behavior of loess, particularly under the unsaturated condition. For instance, loess is found to have very high shear strength under arid condition due to matrix suction and natural cementation (Barden et al., 1973; Dijkstra, 2001; Xu et al., 2018). It can show large collapse compression upon wetting, which is related to the reduction in suction and collapse of the soil structure (Derbyshire, 2001; Dijkstra, 2001; Delage et al., 2005; Sánchez et al., 2005; Mašín, 2017). There has been extensive research on the stress-strain relationship and internal structure of unsaturated loess (Barden et al., 1973, Grabowska-Olszewska, 1975; Derbyshire et al., 1994; Derbyshire, 2001; Dijkstra, 2001; Jiang et al., 2014). It is shown that the natural structure plays an important role in controlling the collapsibility and shear strength of loess under unsaturated conditions (Derbyshire et al., 1994; Wen and Yan, 2014; Rogers et al., 1994; Muñoz-Castelblanco et al., 2011; Garg et al., 2019). But much less attention has been paid to the effect of internal structure on the stress-strain relationship of saturated loess. Recent studies have highlighted the structural effect on thermos-plasticity of saturated loess (Ng et al., 2019; Zhou and Ng, 2018). There are two possible reasons for neglecting the effect of structure on saturated natural loess behavior. Firstly, most of the loess is found in arid and semi-arid areas of the world, where deep layers of unsaturated soils exist. Secondly, it is believed that the loess structure may be completely damaged during the wetting process, and therefore, there should be negligible influence of structure on the mechanical behavior of saturated loess.

Though there is little research on the structural effect on loess behavior after wetting from an unsaturated state, there is abundant experimental evidence that the mechanical response of saturated natural loess

(below the natural ground water table) is dramatically influenced by the structure (Xu and Coop, 2016; Xu et al., 2018; Lu et al., 2019; Cheng et al., 2019; Cheng et al., 2020). Evolution of the soil structure during loading is called destructuration (Rouainia and Muir Wood, 2000). Destructuration causes extra volume contraction, strength reduction and stiffness degradation of the natural soil. Such soil response is of great importance for geotechnical engineering practice. For instance, it is found that some of the landslides in loess is related to not only the collapse compression of unsaturated loess under wetting but also the destructuration of the saturated loess during mechanical loading (Tu et al., 2009; Jiang et al., 2014; Xu et al., 2018). It is therefore of great significance to investigate the effect of the natural structure on mechanical behavior of saturated loess, for understanding the development of deep-seated landslides in saturated loess (Tu et al., 2009; Xu et al., 2018). In addition, a proper constitutive model for natural loess is useful for both interpreting the structural effect on soil response and solving real boundary value problems such as the development of landslides and failure of loess foundations.

As far as authors are aware, very few attempts have been made in modelling the mechanical behavior of natural saturated loess. Liu et al. (2013) have proposed a constitutive model for loess but the model has only been used in simulating the undrained effective stress path of a loess. Its capability in modelling the soil response under other loading conditions has not been verified. Many constitutive models have also been developed for structured soils (e.g. Asaoka et al., 1998, 2000; Asaoka et al., 2000; Zhang et al., 2007; Baudet and Stallebrass, 2004; Huang et al., 2011; Ye and Ye, 2016; Yang et al., 2020; Yin et al., 2011a; Yin et al., 2011b) but are rarely against the mechanical response of natural loess.

In view of the afore-mentioned issues, this study aims to obtain better understanding on the behavior of

saturated natural loess through experiments and constitutive modelling. A series of oedometer and drained triaxial compression tests on both natural (undisturbed) and remolded loess samples have been carried out. The natural samples were obtained in the Loess Plateau of China. Based on the experimental observations, a constitutive model for natural loess is proposed within the theoretical framework of subloading and superloading surface concepts (Asaoka et al., 1998, 2000, 2002; Zhang et al., 2007; Ye and Ye, 2016). An important feature of the model is that it considers the effect of both plastic volumetric and shear strain on destructuration. A new method for determining the initial degree of structure is developed. The proposed model is validated against the experimental results. In the following experimental investigation and constitutive modelling, all the stress quantities are the effective ones.

2. Experiments

2.1. Sample preparation and test setup

Intact loess was sampled from south Loess Plateau of China in Jingyang County, Shaanxi Province (Xu and Coop, 2016), with the aid of a thin-wall tuber. The sampling location is in the platform of a farmland, where the groundwater table is close to the ground level due to long-term irrigation activities. The sampling depth was about 41 m. The loess samples were extracted from the fifth loess layer (L5) belonging to Q2 (Middle Pleistocene epoch) (Fig. 1). All the undisturbed specimens were cut in situ from loess blocks, which were cautiously excavated after clearing the surface soil at least 0.5 m thick. Samples were wrapped by plastic film, put in PVC boxes and then carefully transported to the laboratory. Sawdust was placed between the sample and PVC box to avoid sample damage. There was no history of slope failure at the sampling site. The axial stress is perpendicular to the deposition plane in the triaxial tests of this study. The physical properties of the natural soil are shown in Table 1. The soil mineral constitution is

similar to that of the soil reported in Xu and Coop (2016). The particle size distribution is shown in Fig. 2. The silt content (5~50 μm) is about 72%, clay content (<5 μm) is about 22% and sand content is (>50 μm) 6%. The soil is thus classified as clay with low plasticity (CL).

In order to study the destructuration characteristics of undisturbed saturated loess, the mechanical response of both undisturbed and remolded loess was tested through oedometer and drained triaxial compression tests. The size of each specimen in an oedometer test was 61.8 mm in diameter and 20 mm in height. Each triaxial specimen was 61.8 mm in diameter and 125 mm in height. The soil samples were saturated by increasing the back pressure. Additional K_0-consolidation tests were carried out to determine the K_0 values for undisturbed and remolded soils (Table 1).

2.2. Results of oedometer tests

There were two major objectives for the oedometer tests: (a) investigating the stress-strain relationship and destructuration of undisturbed loess in one-dimensional compression and (b) developing a method to determine the initial degree of structure of undisturbed loess. To achieve the second objective, the remolded loess was loaded and unloaded to make it have similar void ratio e with that of the undisturbed sample at the initial state of oedometer tests ($\sigma_v \approx$13 kPa). More discussion on determination of the initial soil structure will be given in the constitutive modelling section. Since the undisturbed and remolded samples have similar e at the initial state, the difference between their $e - \sigma_v$ curves shown in Fig. 3 is mainly caused by the structure of natural loess. After the initial state, the undisturbed specimen always show a larger void ratio than the remolded specimen under the same σ_v. The two void ratios are getting closer as σ_v increases, due to the progressive damage of the soil structure. It is expected that the structure

of undisturbed specimens would be completely damaged at sufficiently high σ_v, making the $e - \sigma_v$ curve of natural loess merge with the normal consolidation line (NCL) of remolded soil.

2.3. Results of drained triaxial compression tests

Three sets of drained triaxial compression tests were carried out on undisturbed and remolded Jingyang loess under different confining pressure σ_r (300, 400 and 500kPa). Figs. 4-6 show the triaxial test results. Strain hardening response of undisturbed loess is observed in all the tests. There is no obvious peak in most of the $\varepsilon_a - q$ curves, where ε_a is the axial strain and q is the deviatoric stress defined as the difference between axial stress σ_a and confining pressure σ_r. There is slight decrease in q for the natural loess with $\sigma_r = 300$ kPa after at $\varepsilon_a \approx 1\%$. This could be caused by localized failure inside the sample. Were there no imperfection in the sample, continuous strain hardening response would be observed. At the same confining pressure, undisturbed samples show much higher shear stiffness throughout the tests due to their structure. The difference in the initial shear stiffness for undisturbed and remolded soils reduces as σ_r decreases. This is due to the destructuration during the isotropic consolidation. When the confining pressure σ_r is very large, there will no significant damage of the soil structure during the consolidation process. This will make the mechanical response of remolded and undisturbed loess very similar. It is expected that the soil structure would have been completely damaged at the critical state with infinitely large shear strain. It implies that $\varepsilon_a - q$ curves for undisturbed and remolded soils should merge together at large ε_a. But it is extremely difficult to shear the soil to critical state in the laboratory. In this study, the tests were terminated before ε_a reaches 20% due to significant strain localization (either shear band or bulging) in the samples. Generally, the undisturbed samples show more volumetric contraction due to destructuration, except for the tests with σ_r =300 kPa.

3. A constitutive model of saturate loess accounting for destructuration

A new constitutive model is presented to describe the mechanical behavior of natural loess. The model is proposed based on the one developed by Zhang et al. (2007), which accounts for the effect of structure, density and stress-induced anisotropy under cyclic loading on mechanical behavior of clays. Specifically, the destructuration evolution law in Zhang et al., (2007) is modified to better describe the stress-strain relation of saturated natural loess, which considers the effect of plastic shear strain. The structure of natural loess includes both cementation and fabric anisotropy (Rouainia and Muir Wood, 2000). For the same of simplicity, the soil cohesion is not considered in this study.

3.1. Description of the model

In order to describe the effect of density (or overconsolidation) and structure of geomaterials, Asaoka et al. (1998, 2000) and Zhang et al. (2007) incorporated the concepts of subloading and superloading yield surfaces into the framework of critical state soil mechanics (Muir Wood, 1990). A brief description of the normal yielding surface, subloading surface and superloading surface is shown in Fig. 7. The similarity ratio of the superloading surface to the normal yield surface, R^*, and the similarity ratio of the superloading surface to the subloading surface, R, are given as:

$$R = \frac{p}{\bar{p}} = \frac{q}{\bar{q}} = \frac{p_m}{\bar{p}_m} \ (0 < R \leq 1) \ \text{and} \ R^* = \frac{\hat{p}}{\bar{p}} = \frac{\hat{q}}{\bar{q}} = \frac{\hat{p}_m}{\bar{p}_m} \ (0 < R^* \leq 1) \quad (1)$$

where (p, q), $(\hat{p}, \hat{q})$ and $(\bar{p}, \bar{q})$ denote the stress states on the subloading yield surface, normal yield surface and superloading surface, respectively. The current stress state (p, q) always lies on the subloading yields surface, which is inside or the same as the normal yield surface when the soil is overconsolidated or normally consolidated, respectively. The superloading surface is larger than or identical to the normal yield surface for a structured or remodeled soil, respectively. For a remolded and normally consolidated

soil, $R = R^*$=1 and all the three yield surfaces become identical. The stress invariants involved in Eq. (1) are defined as

$$p = \frac{1}{3}\sigma_{ii},\ \bar{p} = \frac{1}{3}\bar{\sigma}_{ii},\ \hat{p} = \frac{1}{3}\hat{\sigma}_{ii} \tag{2}$$

$$q = \sqrt{\frac{3}{2}s_{ij}s_{ij}},\ \bar{q} = \sqrt{\frac{3}{2}\bar{s}_{ij}\bar{s}_{ij}}\ ,\ \hat{q} = \sqrt{\frac{3}{2}\hat{s}_{ij}\hat{s}_{ij}} \tag{3}$$

$$s_{ij} = \sigma_{ij} - p\delta_{ij}\ ,\ \bar{s}_{ij} = \bar{\sigma}_{ij} - \bar{p}\delta_{ij},\ \hat{s}_{ij} = \hat{\sigma}_{ij} - \hat{p}\delta_{ij} \tag{4}$$

where σ_{ij} is the stress tensor, s_{ij} is the deviatoric stress tensor and δ_{ij} (=1 for *i*=*j* and =0 otherwise) is the Kronecker delta tensor.

The expressions for the three yield surfaces are

$$f = \ln\frac{p}{p_m} + \ln\frac{M^2+\eta^{*2}}{M^2} = 0 \tag{5}$$

$$\hat{f} = \ln\frac{\hat{p}}{\hat{p}_m} + \ln\frac{M^2+\hat{\eta}^{*2}}{M^2} = 0 \tag{6}$$

$$\bar{f} = \ln\frac{\bar{p}}{\bar{p}_m} + \ln\frac{M^2+\bar{\eta}^{*2}}{M^2} = 0 \tag{7}$$

where f, $\hat{f}$ and $\bar{f}$ are the expressions for the subloading, normal and superloading yield surfaces, respectively; *M* is critical state stress ratio of remolded soil in triaxial compression; η^* is the anisotropic stress ratio defined as

$$\eta^* = \sqrt{\frac{3}{2}\left(\frac{s_{ij}}{p} - \beta_{ij}\right)\left(\frac{s_{ij}}{p} - \beta_{ij}\right)} \tag{8}$$

where β_{ij} is a tensor for describing the anisotropy, which is expressed as below in triaxial compression

$$\beta_{ij} = \begin{bmatrix}\beta_a & 0 & 0\\ 0 & \beta_r & 0\\ 0 & 0 & \beta_r\end{bmatrix} = \frac{2}{3}\begin{bmatrix}\zeta_0 & 0 & 0\\ 0 & -\zeta_0/2 & 0\\ 0 & 0 & -\zeta_0/2\end{bmatrix} \tag{9}$$

where ζ_0 is the initial variable of anisotropy; β_a and β_r are the components of β_{ij} in the axial and

radial directions, respectively. In the present study, the stress-induced anisotropy is neglected and the anisotropic tensor β_{ij} remains unchanged during loading. Similar to η^*, $\hat{\eta}^*$ and $\bar{\eta}^*$ are expressed as

$$\hat{\eta}^* = \sqrt{\frac{3}{2}\left(\frac{\hat{s}_{ij}}{p} - \beta_{ij}\right)\left(\frac{\hat{s}_{ij}}{p} - \beta_{ij}\right)} \quad \text{and} \quad \bar{\eta}^* = \sqrt{\frac{3}{2}\left(\frac{\bar{s}_{ij}}{p} - \beta_{ij}\right)\left(\frac{\bar{s}_{ij}}{p} - \beta_{ij}\right)} \tag{10}$$

Eq. (5) can be rewritten as below based on the similarity ratios in Eq. (1)

$$f = \ln\frac{M^2+\eta^{*2}}{M^2} + \ln\left(\frac{p}{\hat{p}_m}\frac{\hat{p}_m}{\bar{p}_m}\frac{\bar{p}_m}{p_m}\right) = \ln\frac{M^2+\eta^{*2}}{M^2} + \ln\left(\frac{p}{\hat{p}_m}\frac{R^*}{R}\right) = 0 \tag{11}$$

or

$$f = \ln\left(\frac{M^2+\eta^{*2}}{M^2}p\right) + \ln R^* - \ln R - \ln\hat{p}_m = 0 \tag{12}$$

An associated flow rule is adopted in the model and the plastic strain increment $d\varepsilon_{ij}^p$ is expressed as

$$d\varepsilon_{ij}^p = \langle\Lambda\rangle\frac{\partial f}{\partial\sigma_{ij}} \tag{13}$$

where Λ is the plastic loading index and $\langle\ \ \rangle$ are the McCauley brackets with $\langle\Lambda\rangle = \Lambda$ for Λ>0 and $\langle\Lambda\rangle = 0$ otherwise.

As the anisotropy is assumed to be unchanged in this study, the condition of consistency of the subloading yield surface can be expressed as below based on Eqs. (2)-(4) and (12):

$$df = \frac{\partial f}{\partial\sigma_{ij}}d\sigma_{ij} + \left(\frac{1}{R^*}dR^* - \frac{1}{R}dR - \frac{1}{\hat{p}_m}d\hat{p}_m\right) = 0 \tag{14}$$

In Eq. (14), the latter term describing the evolution of internal structure and plastic hardening $\left(\frac{1}{R^*}dR^* - \frac{1}{R}dR - \frac{1}{\hat{p}_m}d\hat{p}_m\right)$ can be expressed as a product of plastic loading index Λ and plastic modulus h_p. The forms of Λ and h_p will be given later in this section. Isotropic hardening is used for the normal yield surface, with the plastic volumetric strain ε_v^p chosen as the sole internal variable to characterize the evolution of internal structure associated with plastic hardening. The hardening law adopted in the proposed model is identical to that of the Modified Cam-Clay model (Muir Wood, 1990), as follows:

$$d\hat{p}_m = \frac{1}{C_p}\hat{p}_m d\varepsilon_v^p = \langle\Lambda\rangle\frac{1}{C_p}\hat{p}_m\frac{\partial f}{\partial\sigma_{ii}} \tag{15}$$

$$c_p = \frac{\lambda-\kappa}{1+e_0} \tag{16}$$

where $d\varepsilon_v^p$ is the plastic volumetric strain increment, λ is the compression index, κ is the swelling index and e_0 is the initial void ratio.

The evolution law of R in the original model for structured soil is expressed as (Asaoka et al. 2002)

$$dR = U\left\|d\varepsilon_{ij}^p\right\|,\ U = -\frac{mM}{c_p}\ln R \tag{17}$$

where *m* is a positive model parameter determining the evolution rate of overconsolidation and $\left\|d\varepsilon_{ij}^p\right\|$ is expressed as below

$$\left\|d\varepsilon_{ij}^p\right\| = \langle\Lambda\rangle\left\|\frac{\partial f}{\partial\sigma_{ij}}\right\| = \langle\Lambda\rangle\sqrt{\frac{\partial f}{\partial\sigma_{ij}}\frac{\partial f}{\partial\sigma_{ij}}} \tag{18}$$

The evolution equation for the degree of structure, R^*, is given as below in the original model by Asaoka et al. (2002)

$$dR^* = U^*\left\|d\varepsilon_{ij}^p\right\|,\ U^* = \frac{aM}{c_p}R^*(1-R^*) \tag{19}$$

where *a* is a parameter used to control the rate of destructuration.

Assuming that the total strain increment $d\varepsilon_{ij}$ is the summation of the elastic $d\varepsilon_{ij}^e$ and plastic ones $d\varepsilon_{ij}^p$ ($d\varepsilon_{ij} = d\varepsilon_{ij}^e + d\varepsilon_{ij}^p$), one can get the increment of stress tensor $d\sigma_{ij}$ as below based on Eq. (13)

$$d\sigma_{ij} = E_{ijkl}d\varepsilon_{kl}^e = E_{ijkl}\left(d\varepsilon_{kl} - d\varepsilon_{kl}^p\right) = E_{ijkl}\left(d\varepsilon_{kl} - \Lambda\frac{\partial f}{\partial\sigma_{kl}}\right) \tag{20}$$

where E_{ijkl} is the elastic stiffness matrix defined as (Hong et al., 2020)

$$E_{ijkl} = (K - 2G/3)\delta_{ij}\delta_{kl} + G(\delta_{ki}\delta_{lj} + \delta_{li}\delta_{kj}) \tag{21}$$

where G and K denote the elastic shear and bulk modulus, respectively. They are the same as that for the Modified Cam-Clay model, as function of current effective mean stress:

$$K = \frac{p}{\kappa/(1+e_0)} \tag{22}$$

$$G = \frac{3(1-2\nu)}{2(1+\nu)}K \tag{23}$$

where ν is the Poisson's ratio, which is assumed a constant for both undisturbed and remolded soils. No attempt is made in this model to consider the non-linearity of soil stiffness at small strains, because this model is mainly developed for predicting the plastic deformation and the shear strength of saturated loess, where the plastic behavior at large strain dominates.

The plastic loading index Λ can be obtained as below based on Eqs. (14)-(20)

$$\Lambda = \frac{\frac{\partial f}{\partial \sigma_{ab}}E_{abij}}{h_p + \frac{\partial f}{\partial \sigma_{pq}}E_{pqrs}\frac{\partial f}{\partial \sigma_{rs}}} d\varepsilon_{ij} = \Theta_{ij} d\varepsilon_{ij} \tag{24}$$

where the plastic modulus h_p is (Asaoka et al., 2002)

$$h_p = \frac{1}{C_p}\left\{\frac{\partial f}{\partial \sigma_{ii}} - M\left\|\frac{\partial f}{\partial \sigma_{ij}}\right\|\left[a(1-R^*) + \frac{m\ln R}{R}\right]\right\} \tag{25}$$

The constitutive equation for the model can be finally obtained as below based on Eqs. (20) and (24)

$$d\sigma_{ij} = \left(E_{ijkl} - h(\Lambda)E_{ijmn}\frac{\partial f}{\partial \sigma_{mn}}\Theta_{kl}\right)d\varepsilon_{kl} \tag{26}$$

where $h(\Lambda)$ is the Heaviside step function with $h(\Lambda) = 1$ for $\Lambda > 0$, and $h(\Lambda) = 0$ when $\Lambda \leq 0$.

3.2 Modified evolution law of R^*

In the previous research (Asaoka et al. 2002), the damage rate of structure variable R^* is related to the full plastic strain increment tensor $\left\|d\varepsilon_{ij}^p\right\|$, as shown in Eq. (19). To better describe the liquefaction of sand under cyclic load, Zhang et al. (2007) adopted a new evolution equation of R^* in which only the plastic deviatoric strain increment $d\varepsilon_d^p$ is considered. However, the destructuration under loading is inevitably accompanied by plastic volumetric strain $d\varepsilon_v^p$ for undisturbed soils, which is supported by existing

experimental studies (Baudet and Stallebrass, 2004; Callisto and Rampello, 2004). Furthermore, the contribution of $d\varepsilon_v^p$ and $d\varepsilon_d^p$ to structure destruction is different for different soils. Therefore, $d\varepsilon_d^p$ in the destructuration equation has been replaced with the plastic destructuration strain rate $d\varepsilon_s^p$, which simultaneously considers the effect of both $d\varepsilon_d^p$ and $d\varepsilon_v^p$, as proposed by Rouainia and Muir wood (2000). Thus, Eq. (19) becomes

$$dR^* = U^* d\varepsilon_s^p \tag{27}$$

where

$$d\varepsilon_s^p = \sqrt{(1-B)\left(d\varepsilon_v^p\right)^2 + B\left(d\varepsilon_d^p\right)^2} \quad \text{with} \quad d\varepsilon_d^p = \langle \Lambda \rangle \sqrt{\frac{2}{3}\frac{\partial f}{\partial s_{ij}}\frac{\partial f}{\partial s_{ij}}} \tag{28}$$

where B is a parameter used to control the relative contribution of $d\varepsilon_v^p$ and $d\varepsilon_d^p$ to the destructuration rate. The value of parameter B is limited from zero to one. Smaller B means more contribution of $d\varepsilon_v^p$ to the destructuration, and vice versa. For the new model with the modified evolution law for R^*, the complete constitutive equation is still expressed as Eq. (26), but the formulation for h_p needs to be replaced by the equation below:

$$h_p = \frac{1}{C_p}\left\{\frac{\partial f}{\partial \sigma_{ii}} - M\left[a(1-R^*)\sqrt{(1-B)\left(\frac{\partial f}{\partial \sigma_{ii}}\right)^2 + \frac{2}{3}B\left\|\frac{\partial f}{\partial s_{ij}}\right\|^2} + \frac{m\ln R}{R}\left\|\frac{\partial f}{\partial \sigma_{ij}}\right\|\right]\right\} \tag{29}$$

4. Determination of the model parameters and initial state variables

The proposed model includes eight material parameters and three initial state parameters. Five of the model parameters, e_r (void ratio at the reference pressure p_r on the NCL in e-ln$p$ plane for remolded soil), λ, κ, M and v are the same as those in the Modified Cam-clay (MCC) model (Table 2). These five parameters can be determined based on conventional oedometer and triaxial tests results on remolded

loess, following standard procedures (Muir Wood, 1990). In addition to the five MCC model parameters, the rest three new parameters *m*, *a* and *B* should be determined from the test data on undisturbed loess. It is advised to determine the initial values of ζ_0, R_0 and R_0^*, prior to the determination of the three new model parameters. The details of these procedures are presented in the following sections.

4.1 Determination of initial variables $\boldsymbol{\zeta_0}$

The variable ζ_0 describes the initial anisotropy of undisturbed loess. It should be mentioned that the initial fabric of remolded loess is isotropic due to the loading history, and therefore, ζ_0 is 0 for this soil. The value of ζ_0 for undisturbed loess can be estimated approximately according the method proposed by Wheeler et al. (2003) and then adjusted for the best prediction for triaxial compression test data. For a K_0-consolidation test, the following dilatancy can be obtained based on Eqs. (5) and (13)

$$\frac{d\varepsilon_v^p}{d\varepsilon_d^p} = \frac{M^2+(\eta_{u0}-\zeta_0)^2-2\eta_{u0}(\eta_{u0}-\zeta_0)}{2(\eta_{u0}-\zeta_0)} \approx \frac{d\varepsilon_v}{d\varepsilon_d} = \frac{3}{2} \tag{30}$$

where η_{u0} $\left[=\frac{3(1-K_{0u})}{1+2K_{0u}}\right]$ is the stress ratio (q/p) of K_0-consolidated undisturbed samples, with K_{0u} being the lateral earth pressure coefficient. The value of K_{0u} measured in this study is 0.31 (Table 2). Note that the value of ζ_0 determined using Eq. (30) is an approximate one as it assumes that the elastic strain increment is 0. Therefore, it needs to be adjusted for better simulation of the test results. In this study, the value of ζ_0 calculated using Eq. (30) is 1.0, which is then adjusted to capture the strength and dilatancy behavior of undisturbed loess in drained triaxial compression tests (Table 2).

4.2 Size of the initial subloading yield surface $\boldsymbol{p_{m0}}$ and initial variables $\boldsymbol{R_0}$ and $\boldsymbol{R_0^*}$

Since the current stress state always lies on the subloading surface, the initial size of the subloading surface p_{m0} is calculated based on the initial stress state of a test (for both undisturbed and remolded soils) based

on Eq. (5) and Eq. (8), which is expressed as

$$p_{m0} = p_0[M^2 + (\eta_0 - \zeta_0)^2]/M^2 \quad (31)$$

where p_0 and η_0 denote the initial mean stress and initial stress ratio.

The two initial state parameters R_0 and R_0^* represent the initial degree of overconsolidation and structure, respectively. Both can be determined from oedometer tests or isotropic consolidation tests of remolded and undisturbed loess samples. The determination method of R_0 is as following, which is similar to the method in Ye and Ye (2016)

$$R_0 = p_{m0}/\bar{p}_{m0} \quad (32)$$

where p_{m0} is calculated from Eq. (31) and $\bar{p}_{m0}$ denotes the pre-consolidation pressure for the undisturbed soil in isotropic consolidation tests. $\bar{p}_{m0}$ can also be calculated from the oedometer tests for the undisturbed soil using the equations below

$$\bar{p}_{m0} = p_{vu}[M^2 + (\eta_{vu} - \zeta_0)^2]/M^2 \quad (33)$$

$$\eta_{vu} = p_{vu}/q_{vu} \quad (34)$$

where p_{vu} $[= (1 + 2K_{0u})\sigma_{vu}/3]$ and q_{vu} $[= (1 - K_{0u})\sigma_{vu}]$ are the mean and deviatoric stress corresponding to the σ_{vu} and the lateral earth pressure coefficient for undisturbed soil K_{0u}. σ_{vu} (=662kPa) is the pre-consolidation pressure for the undisturbed soil in oedometer tests (the value of σ_v at the maximum curvature point on the $e - \log\sigma_v$ curve for undisturbed loess shown in Fig. 3. The value of $\bar{p}_{m0}$ calculated by Eq. (34) is 528.3 kPa.

The initial structure degree of R_0^* can be determined from the $e - \log\sigma_v$ curves of oedometer tests for the undisturbed and remolded samples which have similar e at the initial state ($\sigma_v \approx 13$ kPa). Because

the remolded loess samples were prepared with the similar void ratio as the natural loess samples before test loading, the difference between their $e - \log\sigma_v$ shown in Fig. 3 is solely caused by the structure and the initial structure degree of R_0^* can be calculated from the pre-consolidation pressure of the undisturbed and remolded samples as following

$$R_0^* = \hat{p}_{m0}/\bar{p}_{m0} \tag{35}$$

where $\bar{p}_{m0}$ is determined by Eq. (33) and $\hat{p}_{m0}$ denotes the pre-consolidation pressure for the remolded soil in isotropic consolidation tests. $\hat{p}_{m0}$ can be calculated based on the $e - \log\sigma_v$ curves of oedometer tests for the remolded samples:

$$\hat{p}_{m0} = p_{vr}[M^2 + \eta_{vr}^2]/M^2 \tag{36}$$

$$\eta_{vr} = p_{vr}/q_{vr} \tag{37}$$

where p_{vr} $[= (1 + 2K_{0r})\sigma_{vr}/3]$ and q_{vr} $[= (1 - K_{0r})\sigma_{vr}]$ are the mean and deviatoric stress corresponding to the σ_{vr} and the lateral earth pressure coefficient for remolded soil K_{0r}. For the remolded loess in this study, $\sigma_{vr} = 111$ kPa (the value of σ_v at the maximum curvature point on the $e - \log\sigma_v$ curve of remolded loess shown in Fig. 3) and $K_{0r} = 0.4$ (Table 1). The value of $\hat{p}_{m0}$ calculated from Eq. (36) is 119.2 kPa.

4.3 Determination of parameters *m*, *a* and *B*

As shown by Ye and Ye (2016), the larger the value of *m*, the larger the curvature of $e - \log\sigma_v$ curve and the larger the value of *a*, the faster the $e - \log\sigma_v$ curve of undisturbed soil revert back to the NCL of remolded soil. Therefore, the values of *m* and *a* can be determined to capture the oedometer tests results for undisturbed loess by assuming that *B*=0.5, because *B* is found to have insignificant influence on the

model prediction for the soil response in such tests (Fig. 8). With the best-tuned parameters of m and a, the parameter B can then be obtained by calibrating the model against the stress-strain relationship in drained triaxial compression tests. Fig. 9 shows the effect of B on the model simulation in drained triaxial tests. It is evident that smaller B results in higher shear stiffness and peak shear strength, but smaller volumetric contraction in drained triaxial compression. This is associated with a slower destructuration rate at a smaller B (R^* increases more slowly with the axial strain ε_a). Finally, the values for m, a and B may have to be fine-tuned to get optimum prediction of the soil response under various loading conditions. But this adjustment is found to be very minor as the influence of B on model simulation in 1D or isotropic compression is insignificant. All the model parameters for Jingyang loess are summarized in Table 2. It is noticed that some advanced methods for parameter identification have been developed (Jin and Yin, 2020; Jin et al., 2020; Yin et al., 2016; Yin et al., 2017). For practical applications, these methods can make the parameter determination more efficient.

5. Model validation

This section presents the validation of the proposed model against the measured compression and shear behavior of both undisturbed and remolded saturated loess from Jingyang, China. Figs. 10-12 show the comparison between the predicted stress-strain relationship and volumetric behavior by the proposed model and the experimental data of undisturbed Jingyang loess. Since the sizes of the initial yield surfaces are determined based on the soil condition at low vertical effective stress, simulations for the triaxial compression tests on natural loess are performed in two steps. First, the soil is loaded in isotropic compression to the confining pressure, during which the structure damage is considered. The soil is then loaded following the stress path in drained triaxial compression. The strain in the figures for triaxial

compression are set to be 0 at the beginning of the triaxial tests (Figs. 10-12). In general, the model gives satisfactory prediction for the test results of undisturbed samples under different confining pressures, with slight overestimation of volumetric contraction at σ_r=300 kPa and σ_r=400 kPa. Figs. 13-15 show the model prediction for remolded loess in triaxial compression. For all the confining pressures, the model tends to overestimate the amount of volumetric contraction. Better model prediction can be achieved by using an improved yield function that is able to produce variable shapes of yield surfaces (Yao et al., 2012; Gao et al., 2017).

The measured and predicted $e - \log\sigma_v$ curves of oedometer tests for the undisturbed and the remolded specimens are compared in Fig. 16. The test data implies that the soil structure is not completely damaged even at $\sigma_v = 4800$ kPa, as the $e - \log\sigma_v$ curve for remolded loess still slightly deviates from that of the undisturbed loess (Figs. 3 and 16).

6. Conclusions

The review of the literature has shown a lack of experimental and theoretical investigation into the structural effects on compression and shear behavior of saturated natural loess. This study presents a series of oedometer and triaxial tests on undisturbed and remolded loess, and a constitutive model for describing the destruction of saturated loess in the light of the experimental evidences. A new simple method for determining the initial degree of structure has been proposed. Based on the experimental investigation and the associated theoretical development, the following conclusions can be drawn:

(a) Destructuration occurs in both oedometer tests (i.e., volumetric change dominates) and triaxial compression tests (i.e., shear strain being much larger than the volumetric strain). Significant

structural effect on the stiffness, shear strength and dilatancy of natural loess is observed. Destructuration occurs as the soil deforms, causing extra volumetric contraction of the soil and reduction of the stiffness.

(b) The experimental data indicate that the destructuration is caused by both plastic volumetric strain and plastic shear strain. An improved destruction law, which considers the contribution of both plastic volumetric strain and plastic shear strain on destructuration, is therefore employed based on existing research. This proposed destruction law is then implemented into a critical state elasto-plastic model with the subloading and superloading surface concept. Comparison between the model prediction and test data shows that the new destructuration law can describe the stress-strain behavior of natural loess satisfactorily.

(c) A new method for determining the initial structure parameter R_0^* is proposed. It is calculated based on the yield stress for remolded and undisturbed soils in oedometer tests. The model validation shows that good prediction of the undisturbed soil response can be obtained using the R_0^* calculated using the new method. This method could also be applicable for other structured fine-grained soils.

The current model assumes that the soil structure is initially anisotropic for natural loess but does not evolve, which may not represent the reality (Rouainia and Wood, 2000; Kobayashi Ichizo et al., 2003; Zhang et al., 2007; Huang et al., 2011; Jiang et al., 2012;Yang et al., 2015; Zhang et al., 2016; Yang et al., 2018). Future work will be done to extend this model for modelling the soil anisotropy evolution.

Acknowledgements

This work was financially supported by National Natural Science Foundation of China (41790442 and 5177922) and Qianjiang Talent Plan (QJD1602028).

References

Asaoka A, Nakano M and Noda T (1998) Super loading yield surface concept for the saturated structured soils. *In Application of Numerical Methods to Geotechnical Problems*. (pp. 233–242). Springer, Vienna.

Asaoka A, Nakano M and Noda T (2000) Superloading yield surface concept for highly structured soil behavior. *Soils and Foundations* 40: 99–110.

Asaoka A, Noda T, Yamada E, et al. (2002) An elasto-plastic description of two distinct volume change mechanisms of soils. *Soils and Foundations* 42: 47–57.

Barden L, McGown A and Collins K (1973) The collapse mechanism in partly saturated soil. *Engineering Geology* 7: 49–60.

Baudet B and Stallebrass S (2004) A constitutive model for structured clays. *Géotechnique* 54: 269–278.

Callisto L and Rampello S (2004) An interpretation of structural degradation for three natural clays. *Canadian Geotechnical Journal* 41: 392–407.

Cheng WC, Xue ZF, Wang L, et al. (2019) Using post-harvest waste to improve shearing behaviour of loess and its validation by multiscale direct shear tests. *Applied Sciences* 9: 5206.

Cheng WC, Li G, Liu N, et al. (2020) Recent massive incidents for subway construction in soft alluvial deposits of Taiwan: a review. *Tunnelling and Underground Space Technology* 96: 103178.

Delage P, Cui YJ and Antoine P (2005) Geotechnical problems related with loess deposits in Northern France. *Proceedings of International Conference on Problematic Soils*, 25–27 May 2005, Eastern Mediterranean University, Famagusta, N. Cyprus.

Derbyshire E (2001) Geological hazards in loess terrain, with particular reference to the loess regions of China. *Earth-Science Reviews 54*: 231–260.

Derbyshire E, Dijkstra TA, Smalley IJ, et al. (1994) Failure mechanisms in loess and the effects of

moisture content changes on remoulded strength. *Quaternary International* 24: 5–15.

Dijkstra TA (2001) Geotechnical thresholds in the Lanzhou loess of China. *Quaternary International* 76: 21–28.

Gao GR (1988) Formation and development of the structure of collapsing loess in China. *Engineering Geology* 25: 235–245.

Gao ZW, Zhao JD and Yin ZY (2017) Dilatancy relation for overconsolidated clay. *International Journal of Geomechanics* 17: *06016035*.

Garg A, Huang H, Kushvaha V, et al. (2019) Mechanism of biochar soil pore-gas-water interaction: gas properties of biochar-amended *sandy* soil at different degrees of compaction using KNN modelling. *Acta Geophysica*, 1–11.

Grabowska-Olszewska B (1975) SEM analysis of microstructures of loess deposits. *Bulletin of the International Association of Engineering Geology* 11: 45–48.

Hashiguchi K (1977) Elastoplastic constitutive laws of granular materials. *Constitutive Equations of Soils*. *Proc. 9th ICFSME, Spec. Session 9*, 73–82.

Hong, Y, Wang, LZ, Zhang, JF, et al. (2020). 3D elastoplastic model for fine-grained gassy soil considering the gas-dependent yield surface shape and stress-dilatancy. *Journal of Engineering Mechanics*, ASCE. 10.1061/(ASCE)EM.1943-7889.0001760.

Huang MS, Liu YH and Sheng DC (2011) Simulation of yielding and stress-stain behavior of Shanghai soft clay. *Computers and Geotechnics* 38: 341–353.

Jiang JH, Ling HI and Kaliakin VN (2012) An associative and non-associative anisotropic bounding surface model for clay. *Journal of Applied Mechanics*, 79: 1–10.

Jiang MJ, Zhang FG, Hu HJ, et al. (2014) Structural characterization of natural loess and remolded loess

under triaxial tests. *Engineering Geology* 181: 249–260.

Jin Y and Yin ZY (2020) Enhancement of backtracking search algorithm for identifying soil parameters. *International Journal for Numerical and Analytical Methods in Geomechanics* Epub ahead of print 24 February 2020. DOI:10.1002/nag.3059.

Jin Y, Yin ZY, Zhou WH, et al. (2020) Intelligent model selection with updating parameters during staged excavation using optimization method. *Acta Geotechnica* Epub ahead of print February 2020. DOI: 10.1007/s11440-020-00936-6

Kobayashi I, Soga K, Iizuka A, et al. (2003) Numerical interpretation of a shape of yield surface obtained from stress probe tests. *Soils and Foundations* 43: 95–103.

Kumar H, Ganesan SP, Bordoloi S, et al. (2019) Erodibility assessment of compacted biochar amended soil for geo-environmental *applications*. *The Science of the Total Environment* 672: 698–707.

Liu MD, Liu J, *Horpibulsuk* S, et al. (2013) Simulating the stress and strain behavior of loess via SCC model. *Proceedings of the18th Southeast Asian Geotechnical and Inaugural AGSSEA Conference*, *29 – 31 May 2013, Singapore*.

Lu J, Wang TH, Cheng WC, et al. (2019) Permeability anisotropy of loess under influence of dry density and freeze-thaw cycles. *International Journal of Geomechanics* 19: 04019103.1-04019103.12.

Mašín D (2017) Coupled thermohydromechanical double-structure model for expansive soils. Journal of Engineering Mechanics 143: *04017067*.

Muñoz-Castelblanco J, Delage P, Pereira JM, et al. (2011) Some aspects of the compression and collapse behaviour of an *unsaturated* natural loess. *Géotechnique Letters* 1: 17–22.

Ng CWW, Mu QY and Zhou C (2019) Effects of specimen preparation method on the volume change of clay under cyclic thermal loads. *Géotechnique* 69: 146–150.

Rogers CDF, Dijkstra TA and Smalley IJ (1994) Hydroconsolidation and subsidence of loess: studies from China, Russia, North America and Europe: in memory of Jan Sajgalik. *Engineering Geology* 37: 83–113.

Rouainia M and Wood DM (2000) A kinematic hardening constitutive model for natural clays with loss of structure. *Géotechnique* 50: 153–164.

Sánchez M, Gens A, Guimarães LD, et al. (2005) A double structure generalized plasticity model for expansive materials. *International Journal for Numerical and Analytical Methods in Geomechanics* 29: 751–787.

Tu XB, Kwong AKL, Dai FC, et al. (2009) Field monitoring of rainfall infiltration in a loess slope and analysis of failure mechanism of rainfall-induced landslides. *Engineering Geology* 105: 134–150.

Wheeler SJ, Näätänen A, Karstunen M, et al. (2003) An anisotropic elastoplastic model for soft clays. *Canadian Geotechnical Journal* 40: 403–418.

Wen BP and Yan YJ (2014) Influence of structure on shear characteristics of the unsaturated loess in Lanzhou, China. *Engineering Geology*, *168*: 46–58.

Wood DM (1990) Soil behaviour and critical state soil mechanics. *Cambridge: Cambridge University Press.* doi:10.*1017*/CBO9781139878272.

Xu L and Coop MR (2016) Influence of structure on the behavior of a saturated clayey loess. *Canadian Geotechnical Journal* 53: 1026–1037.

Xu L, Coop MR, Zhang MS, et al. (2018) The mechanics of a saturated silty loess and implications for landslides. *Engineering Geology 236*: 29–42.

Yang C, Sheng DC, Carter JP, et al. (2015) Modelling the plastic anisotropy of Lower Cromer Till. *Computers and Geotechnics* 69: 22–37.

Yang J, Yin ZY, Liu XF, et al. (2020). Numerical analysis for the role of soil properties to the load transfer in clay foundation due to the traffic load of the metro tunnel. *Transportation Geotechnics* 23: 100336.

Yang ZX, Xu TT and Chen YN (2018) Unified modeling of the influence of consolidation conditions on monotonic soil response considering *fabric* evolution. *Journal of Engineering Mechanics* 144: 04018073.

Yao YP, Gao ZW, Zhao JD, et al. (2012) Modified UH model: constitutive modeling of overconsolidated clays based on a parabolic Hvorslev *envelope*. *Journal of Geotechnical and Geoenvironmental Engineering* 138: 860–868.

Ye GL and Ye B (2016) Investigation of the overconsolidation and structural behavior of Shanghai clays by element testing and *constitutive* modeling. *Underground Space* 1: 62–77.

Yin ZY, Hattab M and Hicher PY (2011a) Multiscale modeling of a sensitive marine clay. *International Journal for Numerical and Analytical Methods in Geomechanics* 35: 1682-1702.

Yin ZY, Karstunen M, Chang CS, et al. (2011b) Modeling time-dependent behavior of soft sensitive clay. *Journal of Geotechnical and Geoenvironmental Engineering* 137: 1103 – 1113.

Yin ZY, Jin YF, Shen SL, et al. (2016) An efficient optimization method for identifying parameters of soft structured clay by an *enhanced* genetic algorithm and elastic-viscoplastic model. *Acta Geotechnica* 12:849 – 867.

Yin ZY, Jin YF, Shen JS, et al. (2017) Optimization techniques for identifying soil parameters in geotechnical engineering: *Comparative* study and enhancement. *International Journal for Numerical and Analytical Methods in Geomechanics* 42:70–94.

Zhang F, Ye B, Noda T, et al. (2007) Explanation of cyclic mobility of soils: approach by stress-induced anisotropy. *Soils and Foundations* 47: 635–648.

Zhang H, Chen QS, Chen JJ, et al. (2016) Unified expression of rotational hardening in clay plasticity. *International Journal of Geomechanics* 16: 06016004.

Zhou C and Ng CWW (2018) A new thermo-mechanical model for structured soil. *Géotechnique* 68: 1109–1115.

List of Tables

Table 1 Physical properties of Jingyang loess (L5)

Physical property	Value
Specific gravity, G_s	2.71
Initial dry density, ρ_d (g/cm^3)	1.6
Natural water content, w (%)	11.3
Liquid limit, w_L (%)	28.8
Plastic limit, w_p (%)	19.3
Lateral earth pressure coefficient K_0 (remolded)	0.40
Lateral earth pressure coefficient K_0 (undisturbed)	0.31

Table 2 Initial state and model parameters for Jingyang loess (L5)

Parameter	Value
Compression index, λ	0.102
Swelling index, κ	0.011
Critical state stress ratio in triaxial compression, M	1.13
Poisson's ratio, v	0.31
Reference void ratio, e_r (e at p = 100kPa on NCL of remolded soil in the e-ln$p$ plane)	0.68
Degradation parameter of overconsolidation state, m	10.0
Degradation parameter of structure, a	0.75
Scale parameter for structure degradation, B	0.50
Pre-consolidation pressure of remolded/undisturbed soils in oedometer tests, σ_{vr}/σ_{vu} (kPa)	111 / 662
Initial variable of anisotropy, ζ_0	0.50

List of Figures

Figure 12 Model prediction of the stress-strain relationship of undisturbed Jingyang loess (L5) in drained triaxial compression with σ_r=500 kPa: (a) $\varepsilon_a - q$ relationship; (b) $\varepsilon_a - \varepsilon_v$ relationship

Figure 13 Model prediction of the stress-strain relationship of remolded Jingyang loess (L5) in drained triaxial compression with σ_r=300 kPa: (a) $\varepsilon_a - q$ relationship; (b) $\varepsilon_a - \varepsilon_v$ relationship

Figure 14 Model prediction of the stress-strain relationship of remolded Jingyang loess (L5) in drained triaxial compression with σ_r=400 kPa: (a) $\varepsilon_a - q$ relationship; (b) $\varepsilon_a - \varepsilon_v$ relationship

Figure 15 Model prediction of the stress-strain relationship of remolded Jingyang loess (L5) in drained triaxial compression with σ_r=500 kPa: (a) $\varepsilon_a - q$ relationship; (b) $\varepsilon_a - \varepsilon_v$ relationship

Figure 16 Model prediction of the oedometer tests on (a)undisturbed Jingyang loess (L5) and (b) remolded Jingyang loess (L5).

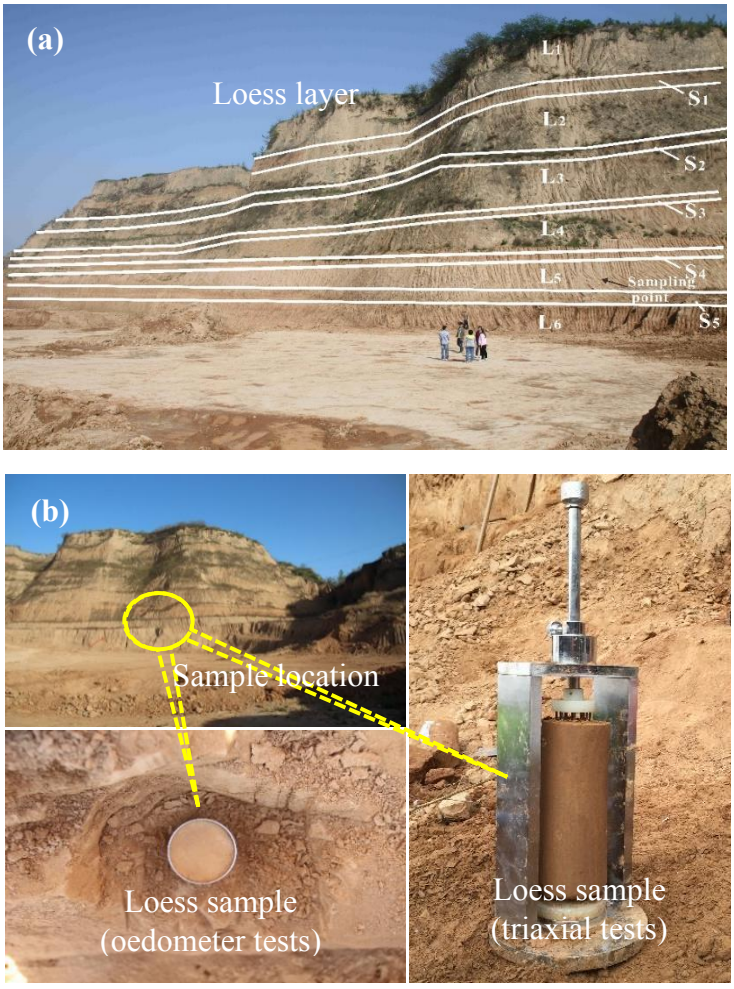
(a)
Loess layer
L1
S1
L2
S2
L3
S3
L4
S4
L5
Sampling point
L6
S5
(b)
Sample location
Loess sample
(oedometer tests)
Loess sample
(triaxial tests)

Fig. 1

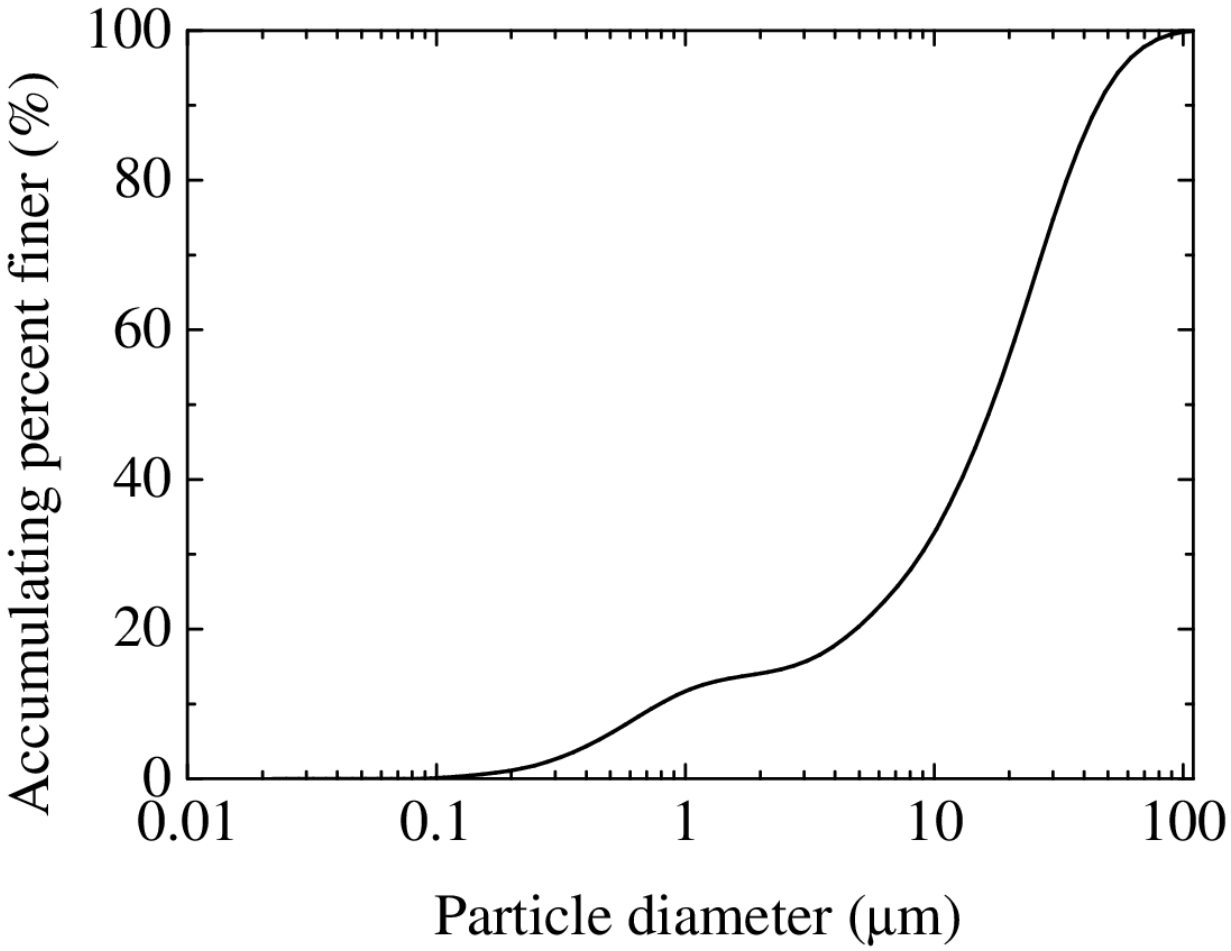
Accumulating percent finer (%)
100
80
60
40
20
0
0.01
0.1
1
10
100
Particle diameter (μm)

Fig.2

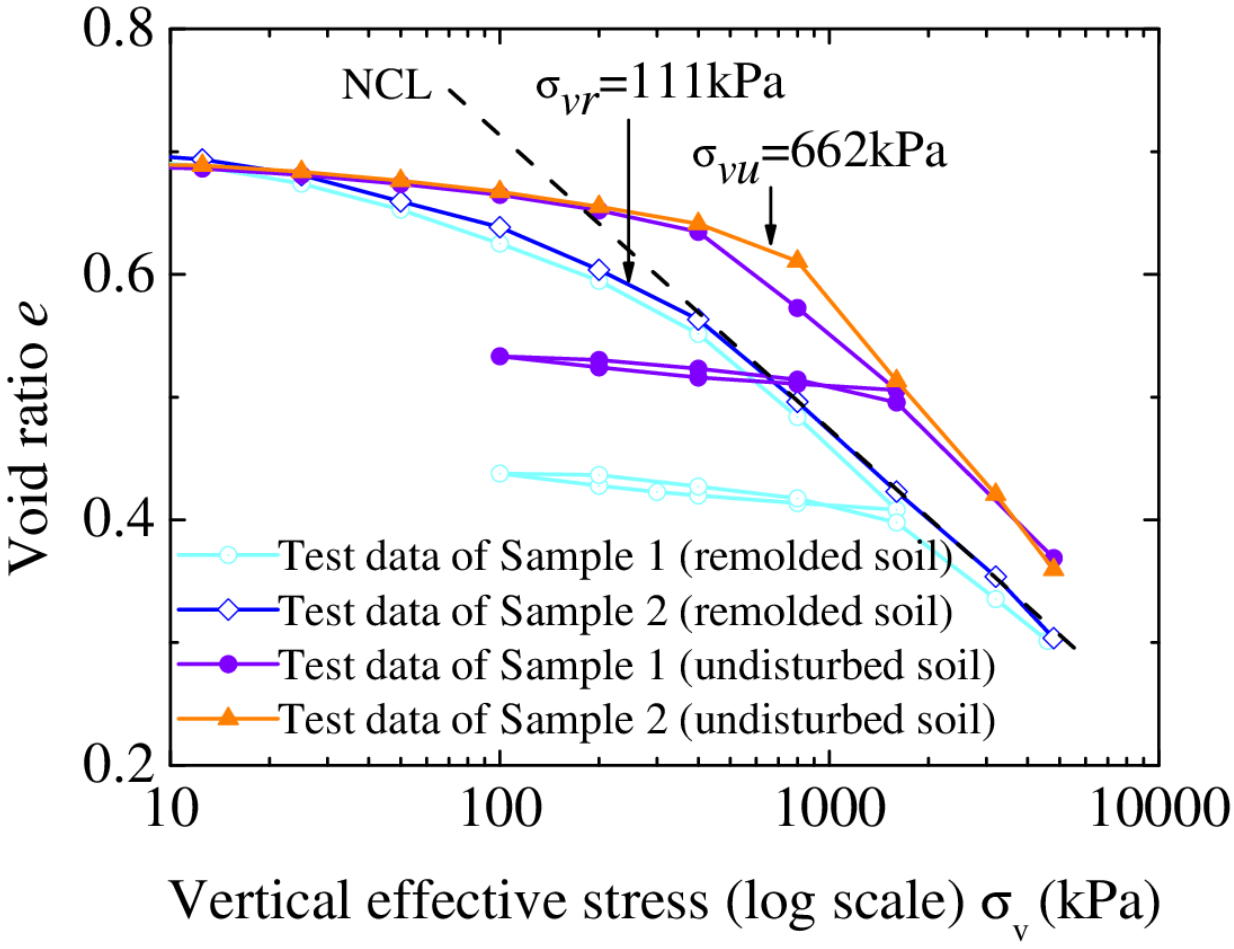
0.8
0.6
0.4
0.2
Void ratio e
NCL
σvr=111kPa
σvu=662kPa
Test data of Sample 1 (remolded soil)
Test data of Sample 2 (remolded soil)
Test data of Sample 1 (undisturbed soil)
Test data of Sample 2 (undisturbed soil)
10
100
1000
10000
Vertical effective stress (log scale) σv (kPa)

Fig. 3

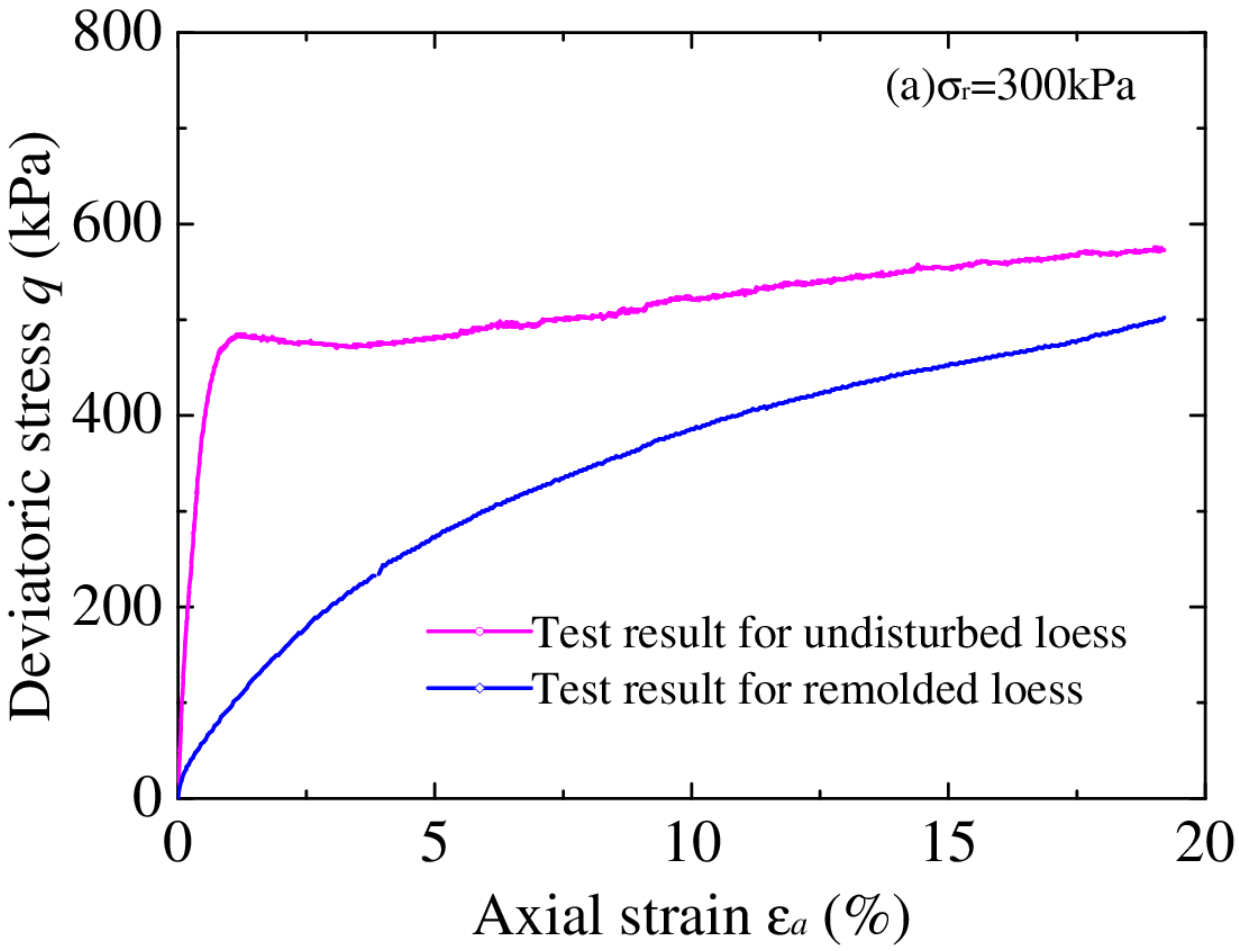
800
600
400
200
0
0
5
10
15
20
(a)σr=300kPa
Deviatoric stress q (kPa)
Axial strain εa (%)
Test result for undisturbed loess
Test result for remolded loess

Fig. 4a

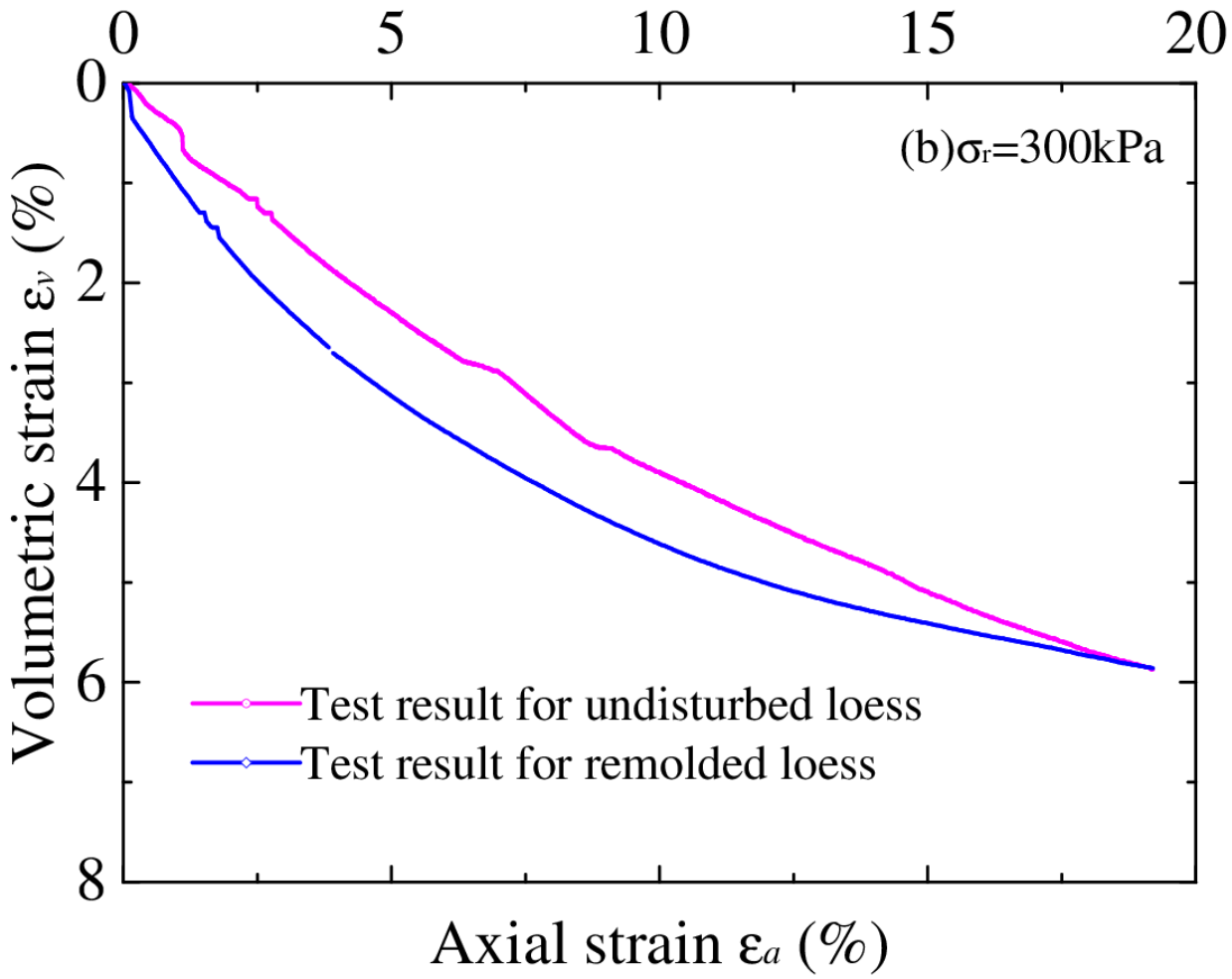
0
5
10
15
20
0
2
4
6
8
(b)σr=300kPa
Volumetric strain εv (%)
Test result for undisturbed loess
Test result for remolded loess
Axial strain εa (%)

Fig. 4b

92

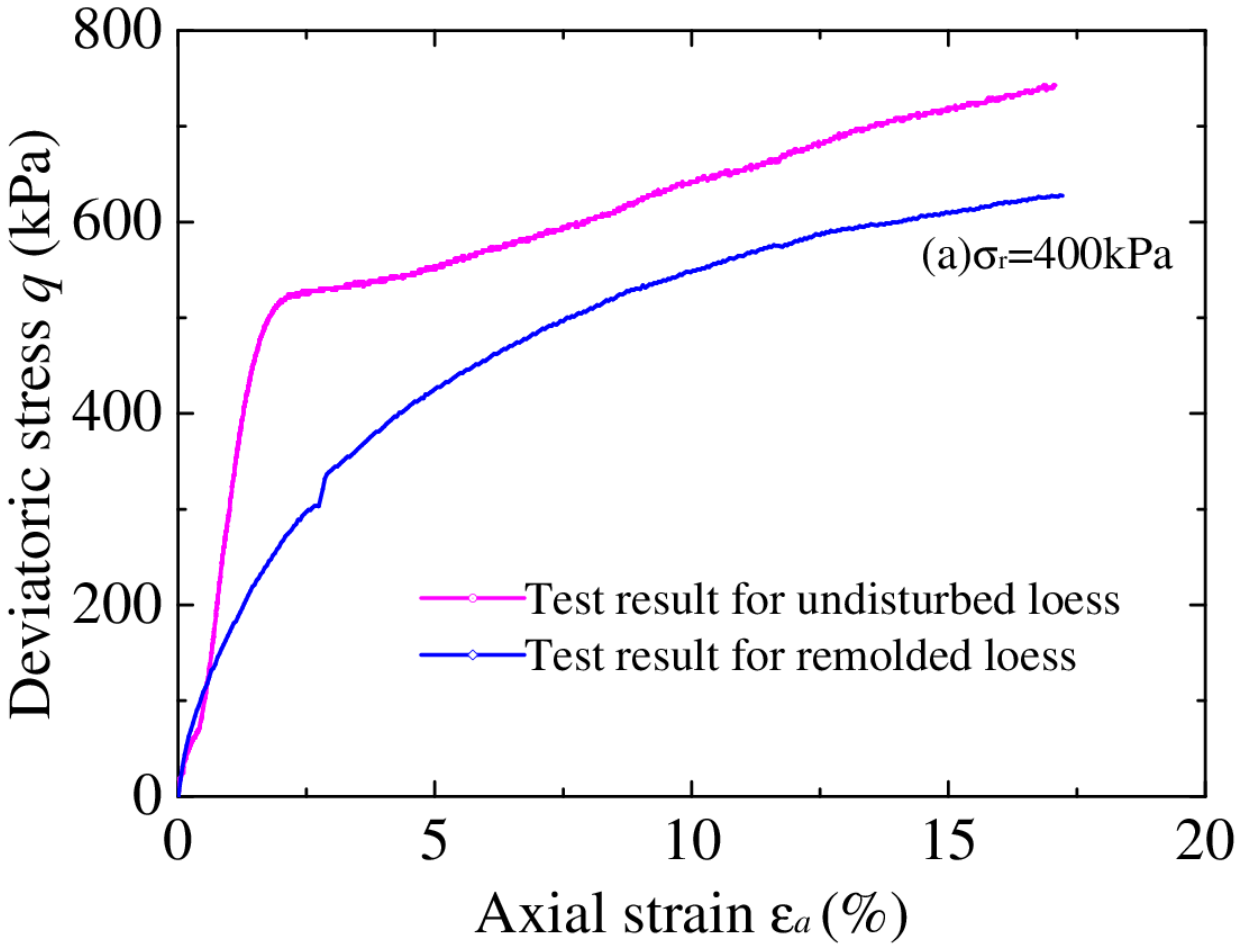
800
600
400
200
0
Deviatoric stress q (kPa)
0
5
10
15
20
Axial strain εa (%)
(a)σr=400kPa
Test result for undisturbed loess
Test result for remolded loess

93

Fig. 5a

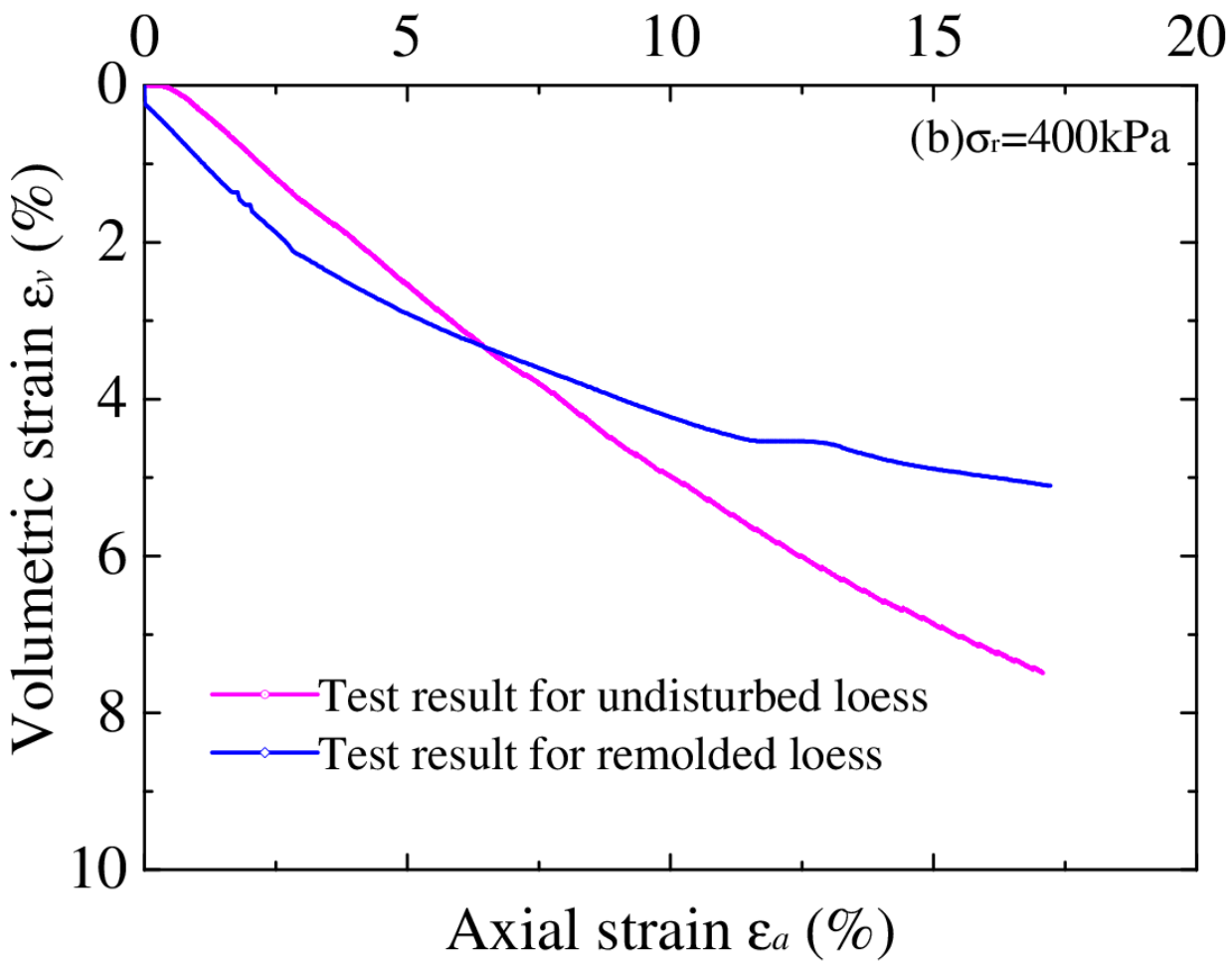
0
5
10
15
20
0
2
4
6
8
10
(b)σr=400kPa
Volumetric strain εv (%)
Axial strain εa (%)
Test result for undisturbed loess
Test result for remolded loess

Fig. 5b

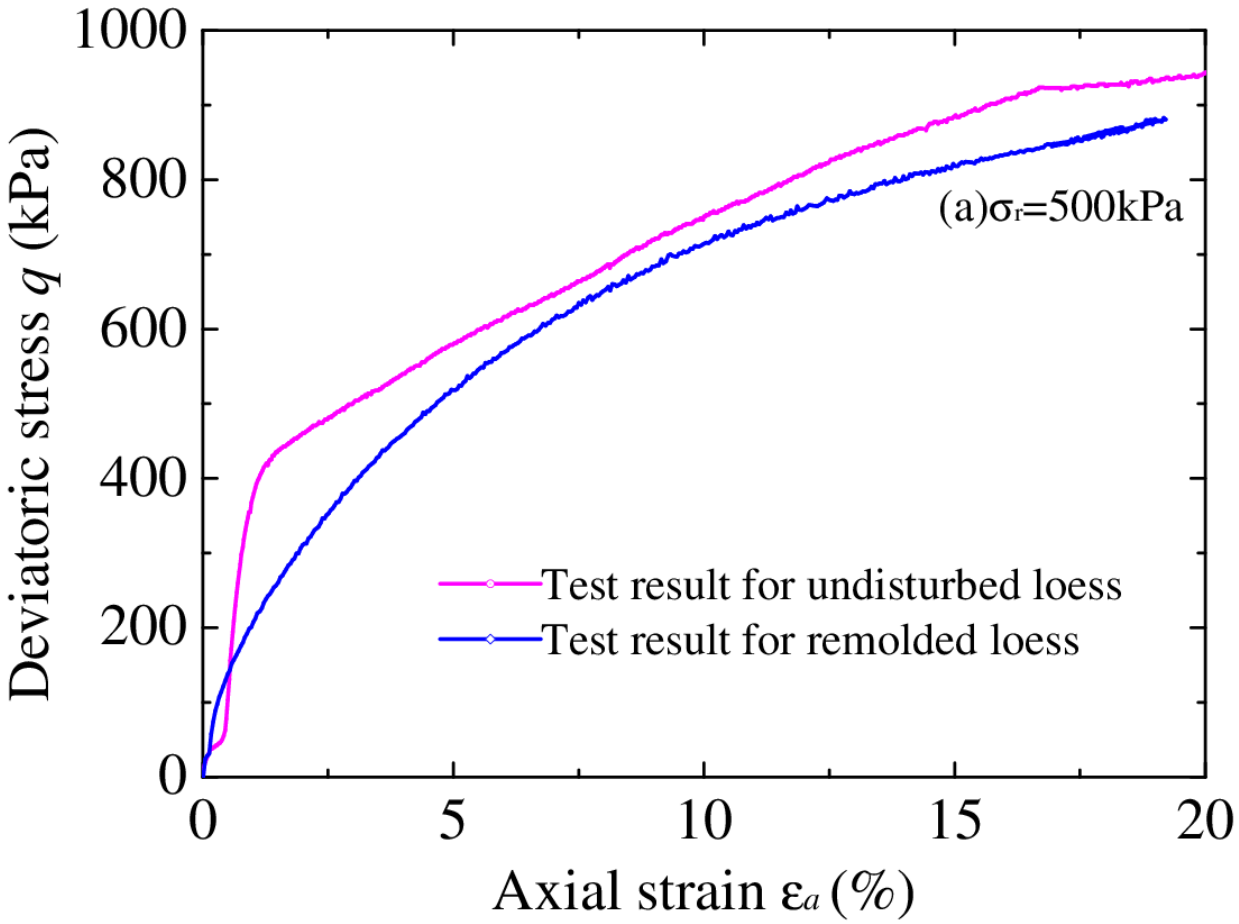
1000
800
600
400
200
0
Deviatoric stress q (kPa)
0
5
10
15
20
Axial strain εa (%)
(a)σr=500kPa
Test result for undisturbed loess
Test result for remolded loess

Fig. 6a

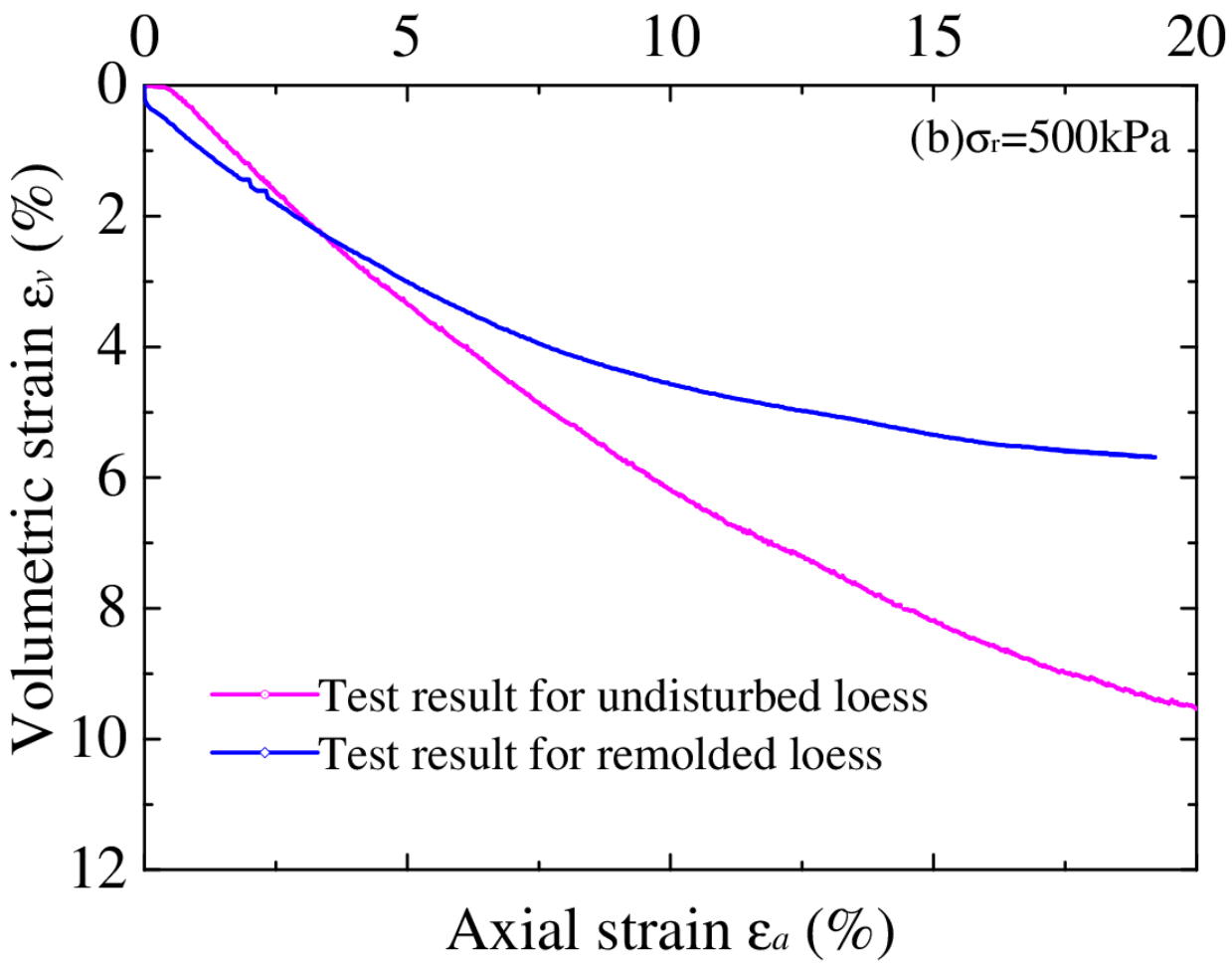
0
5
10
15
20
0
2
4
6
8
10
12
(b)σr=500kPa
Volumetric strain εv (%)
Axial strain εa (%)
Test result for undisturbed loess
Test result for remolded loess

Fig. 6b

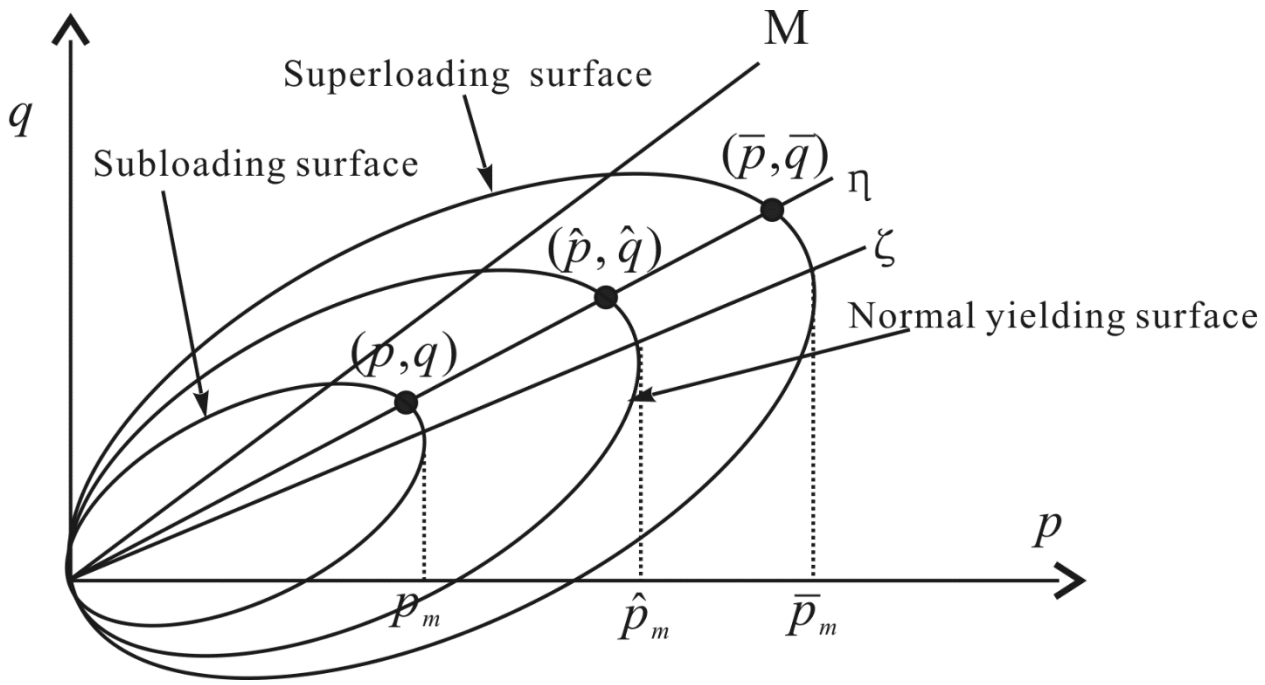
M
Superloading surface
q
Subloading surface
$(\bar{p},\bar{q})$
η
$(\hat{p},\hat{q})$
ζ
Normal yielding surface
(p,q)
p
p_m
$\hat{p}_m$
$\bar{p}_m$

Fig. 7

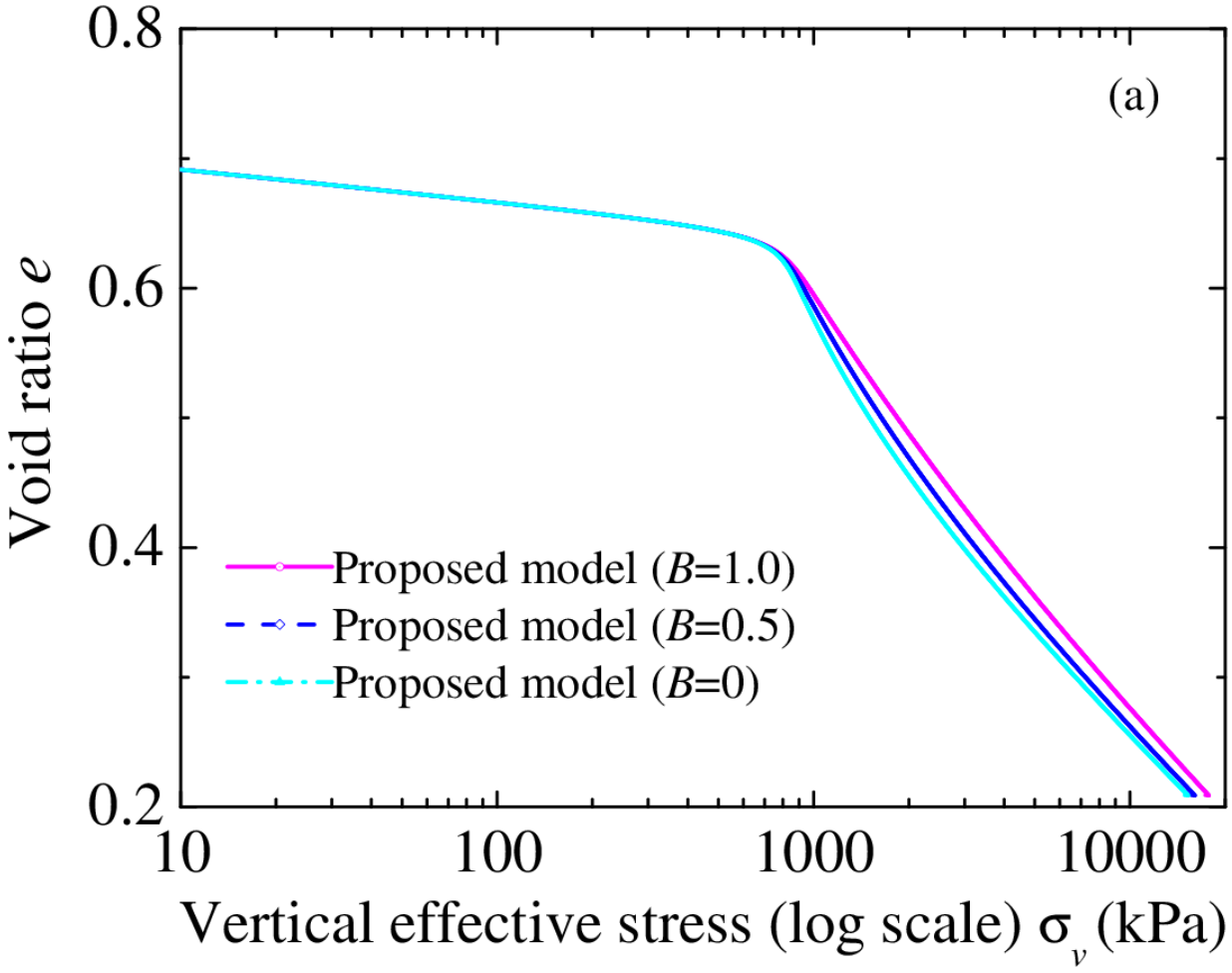

103

104

Fig. 8a

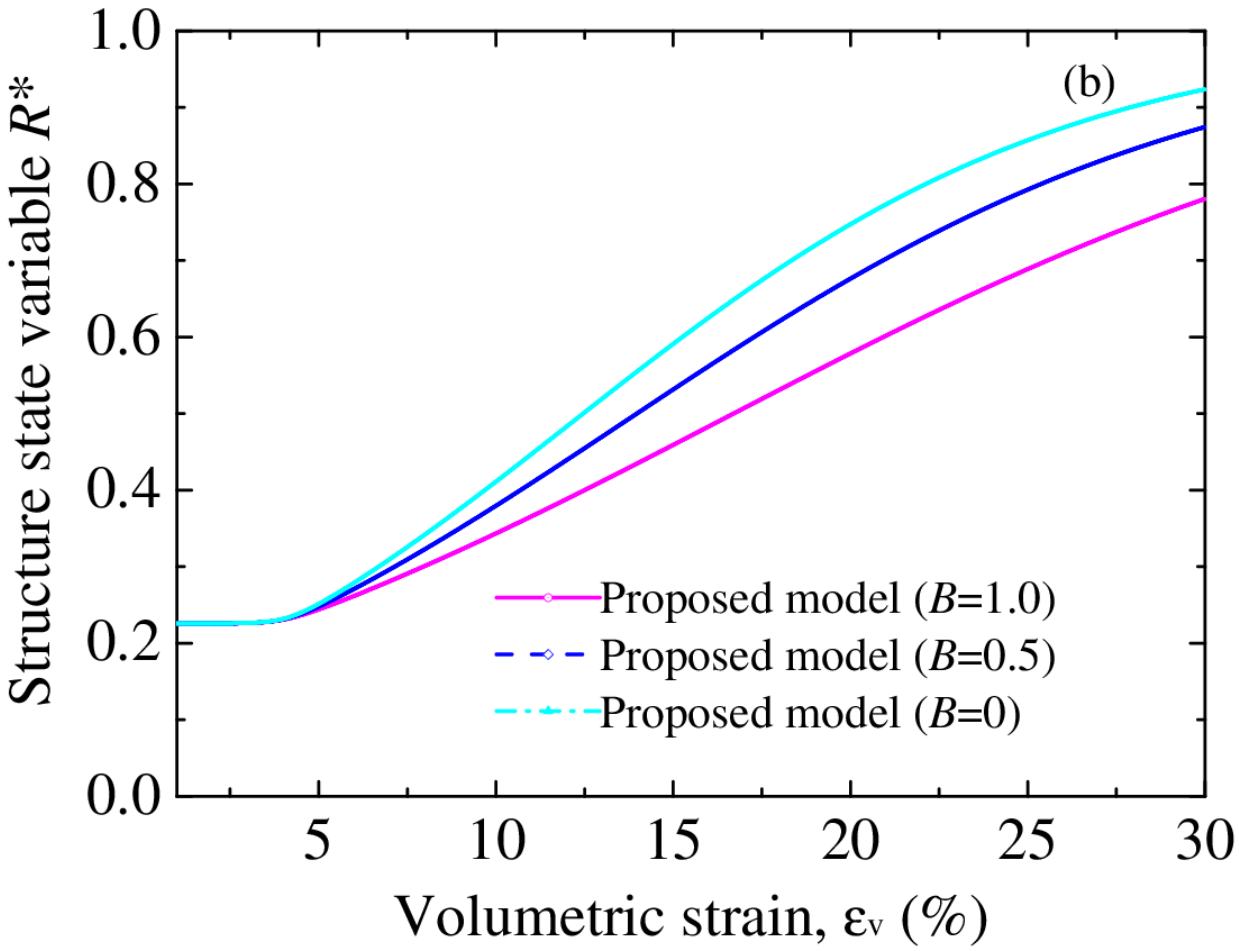
(b)
Structure state variable R*
1.0
0.8
0.6
0.4
0.2
0.0
5
10
15
20
25
30
Volumetric strain, εv (%)
Proposed model (B=1.0)
Proposed model (B=0.5)
Proposed model (B=0)

Fig. 8b

107

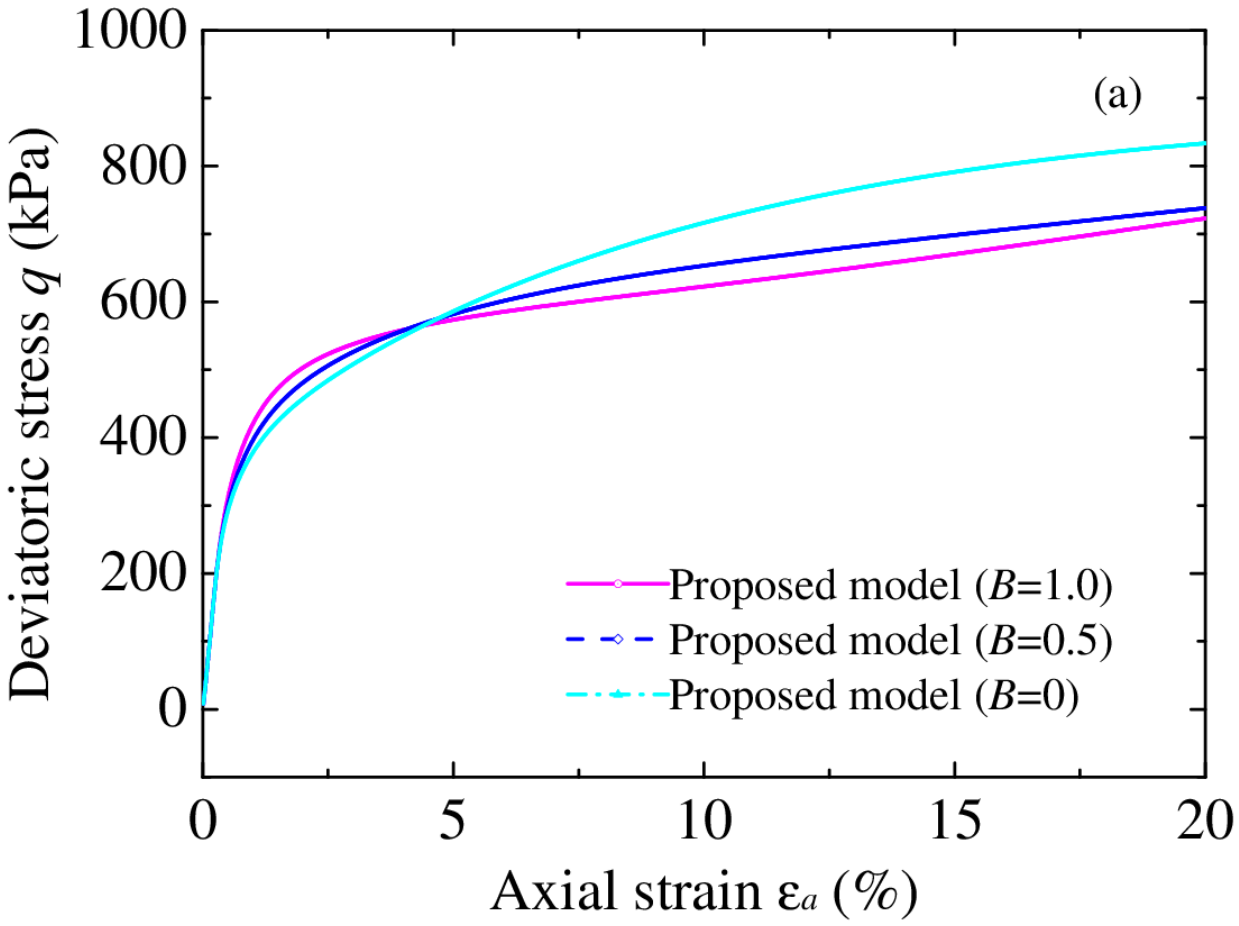

108

Fig. 9a

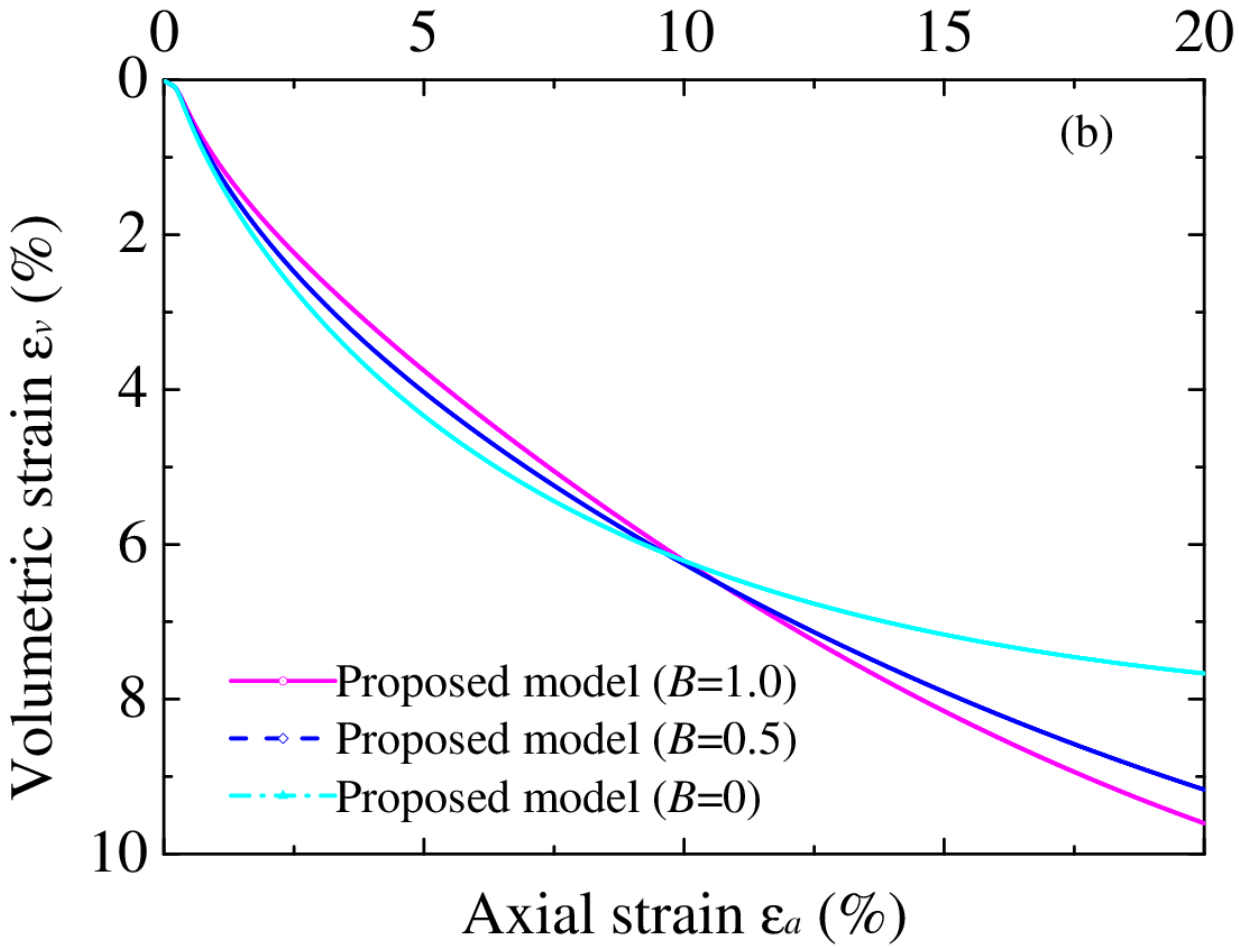
0
5
10
15
20
0
2
4
6
8
10
(b)
Volumetric strain ε_v (%)
Axial strain ε_a (%)
Proposed model (B=1.0)
Proposed model (B=0.5)
Proposed model (B=0)

Fig. 9b

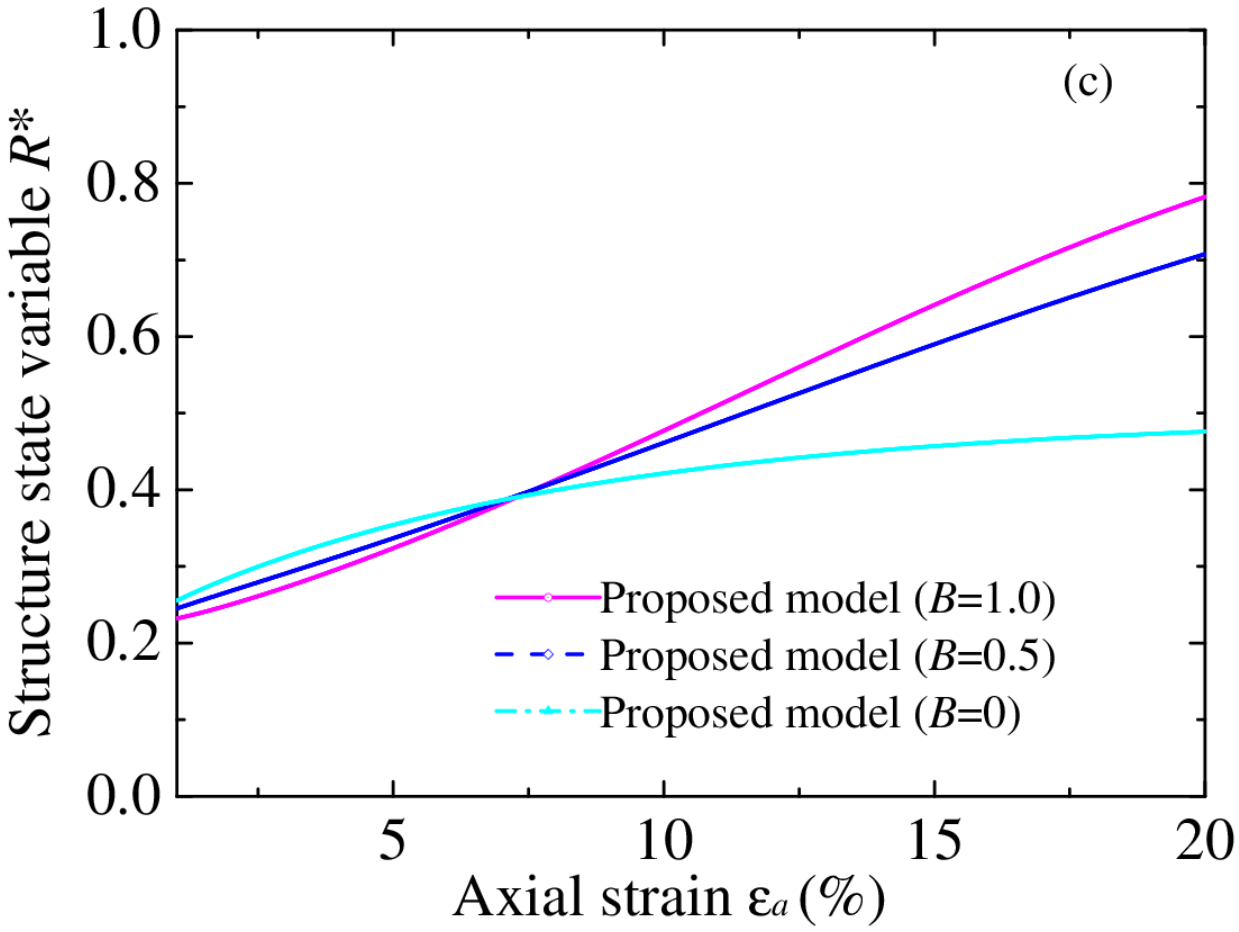
(c)
Structure state variable R^*
1.0
0.8
0.6
0.4
0.2
0.0
5
10
15
20
Axial strain ε_a (%)
Proposed model (B=1.0)
Proposed model (B=0.5)
Proposed model (B=0)

Fig. 9c

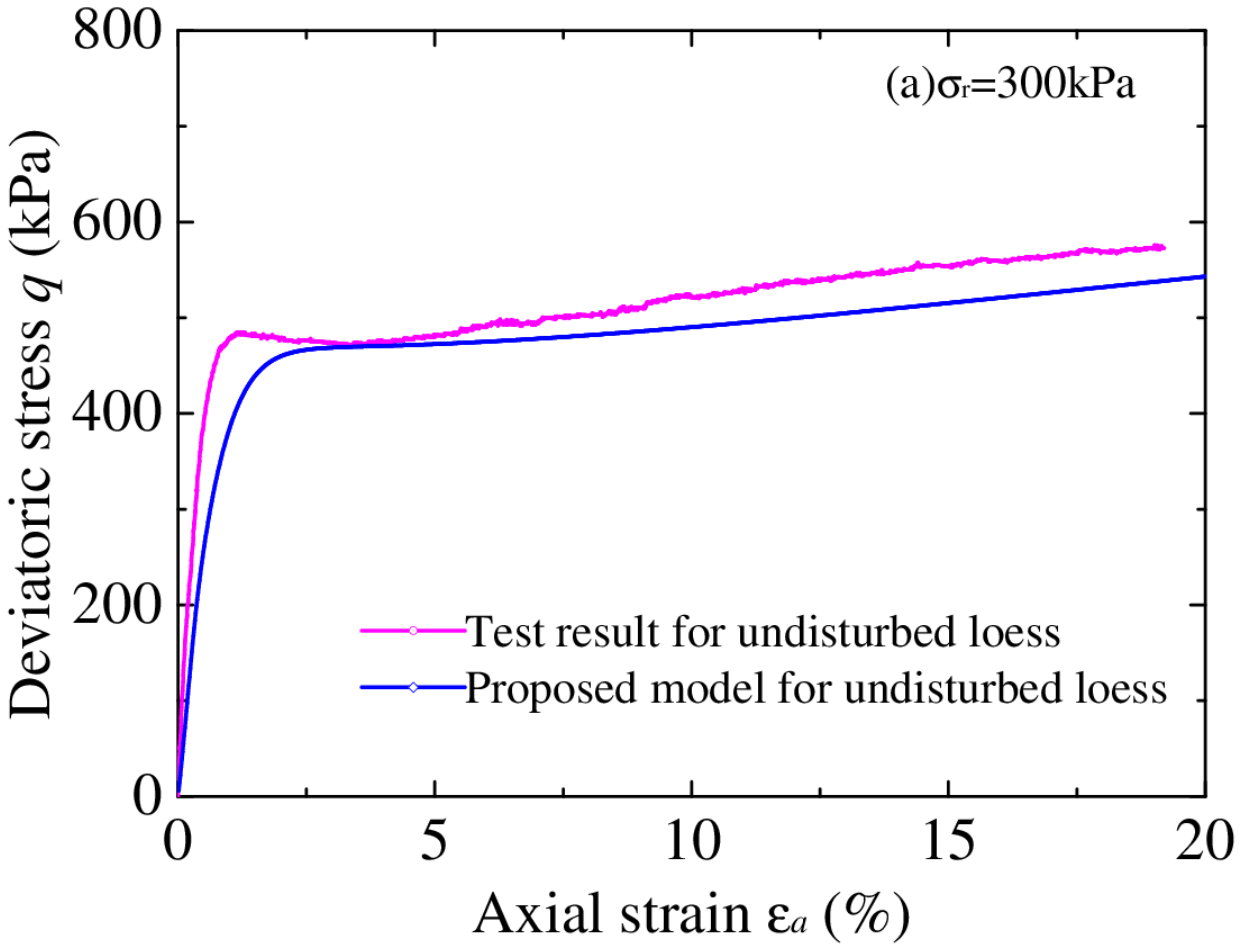

113

114

Fig. 10a

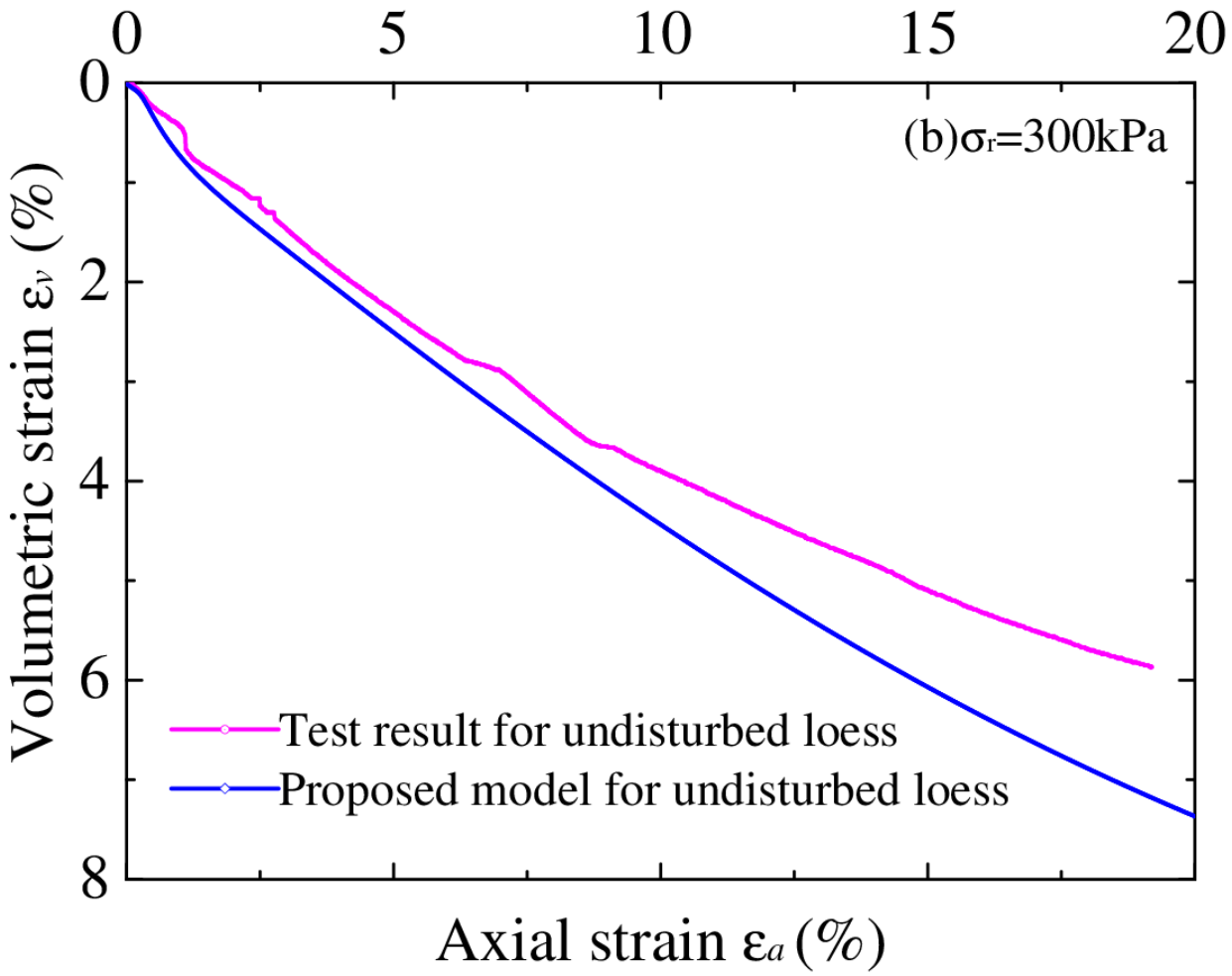

115

116

Fig. 10b

117

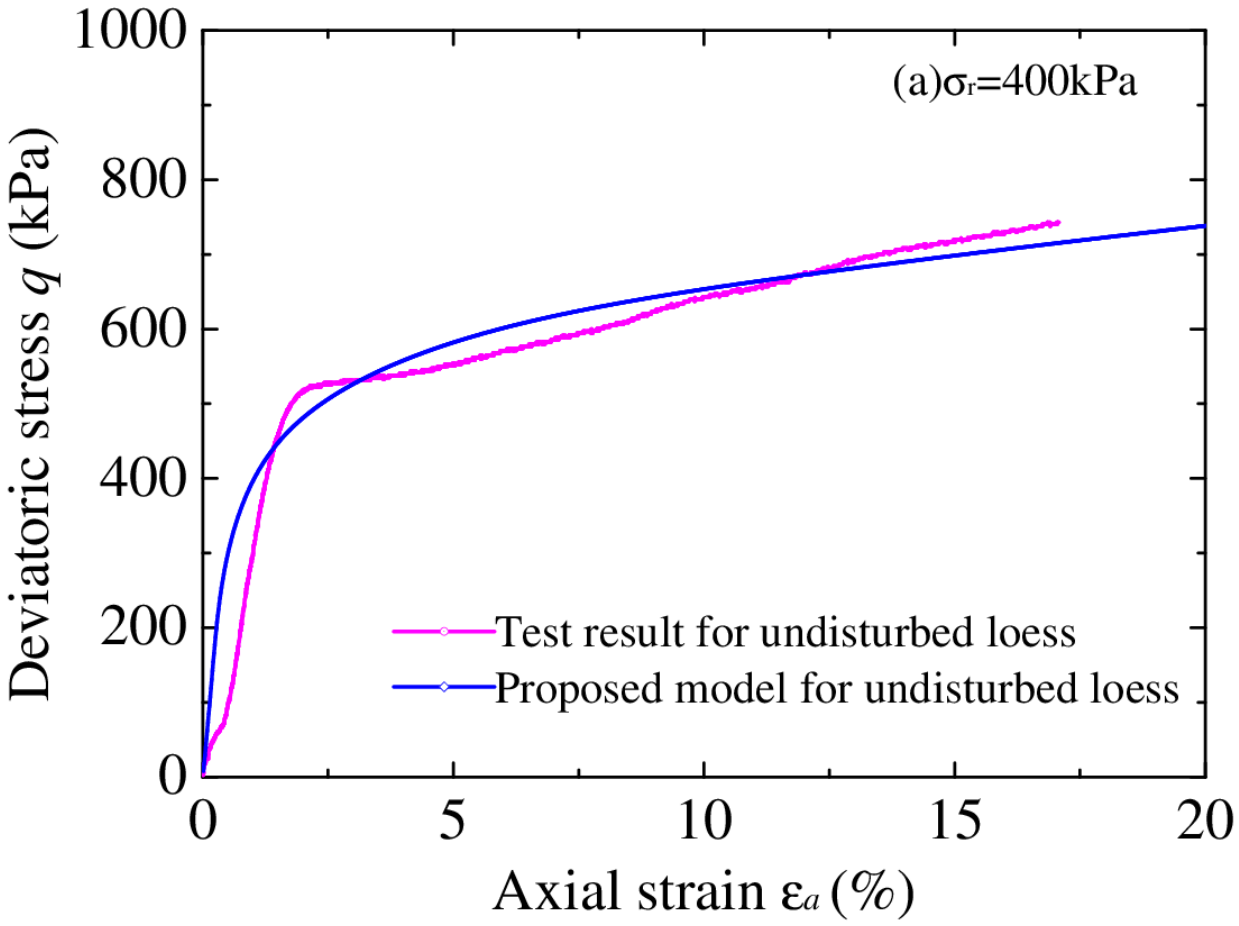

118

Fig. 11a

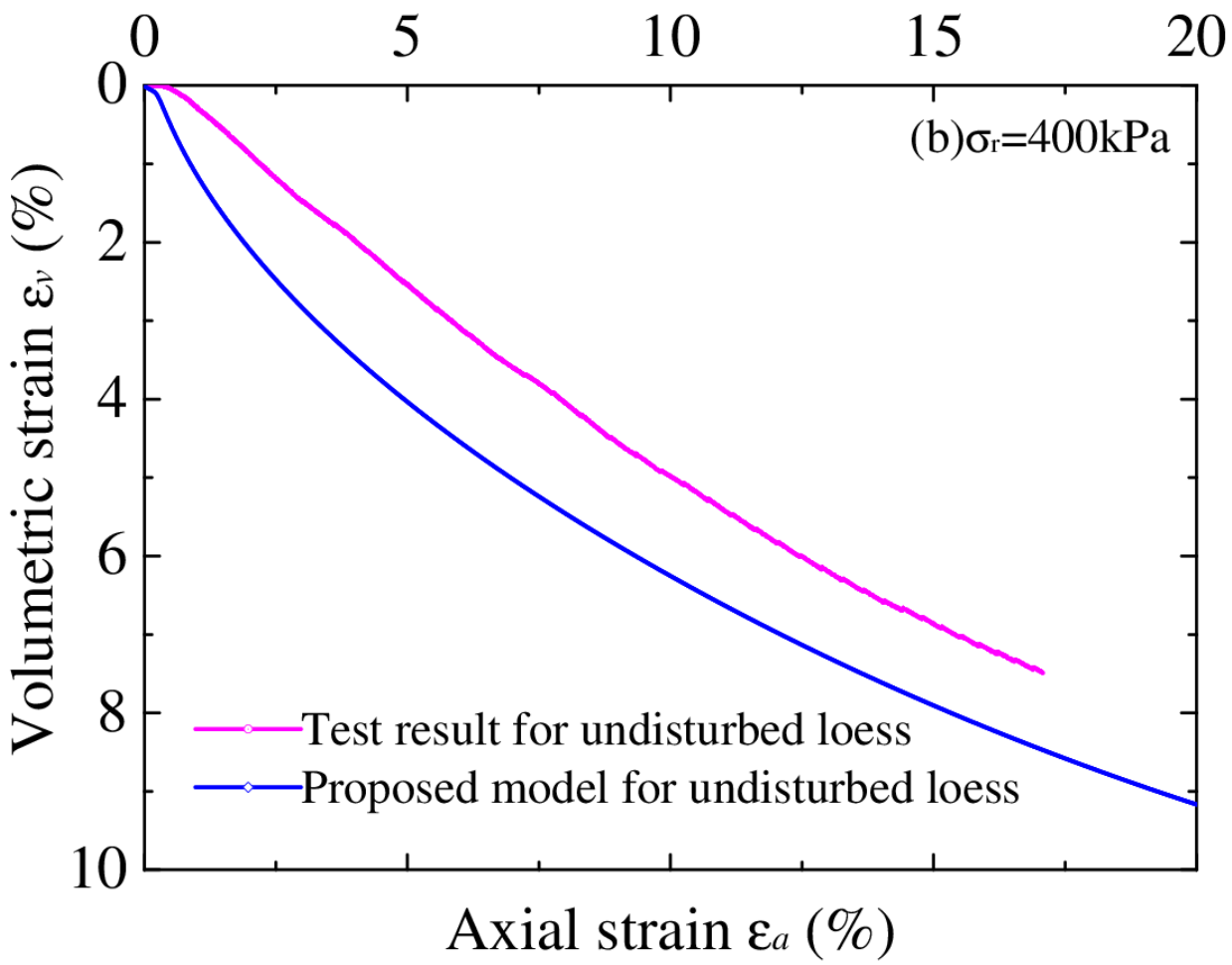

119

120

Fig. 11b

121

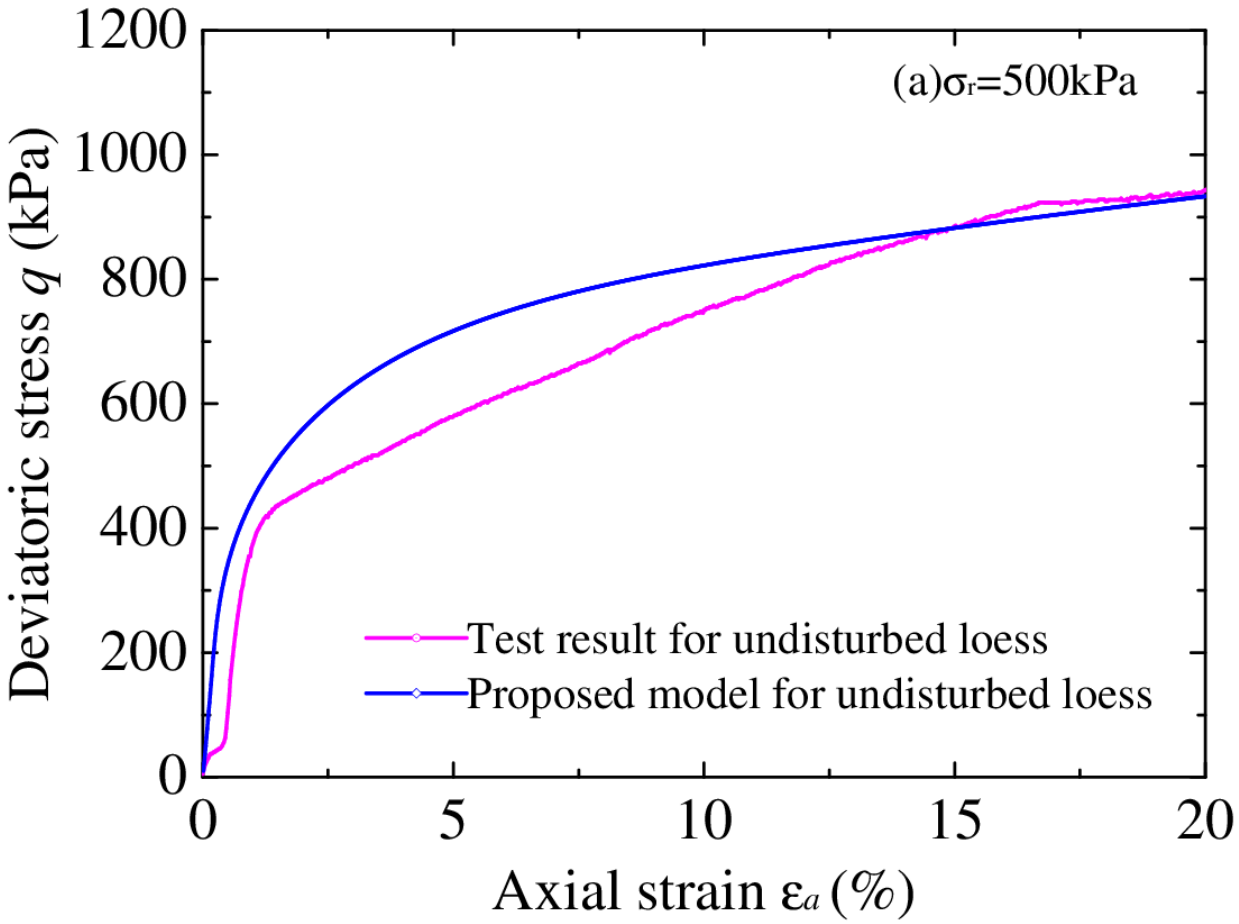

122

Fig. 12a

123

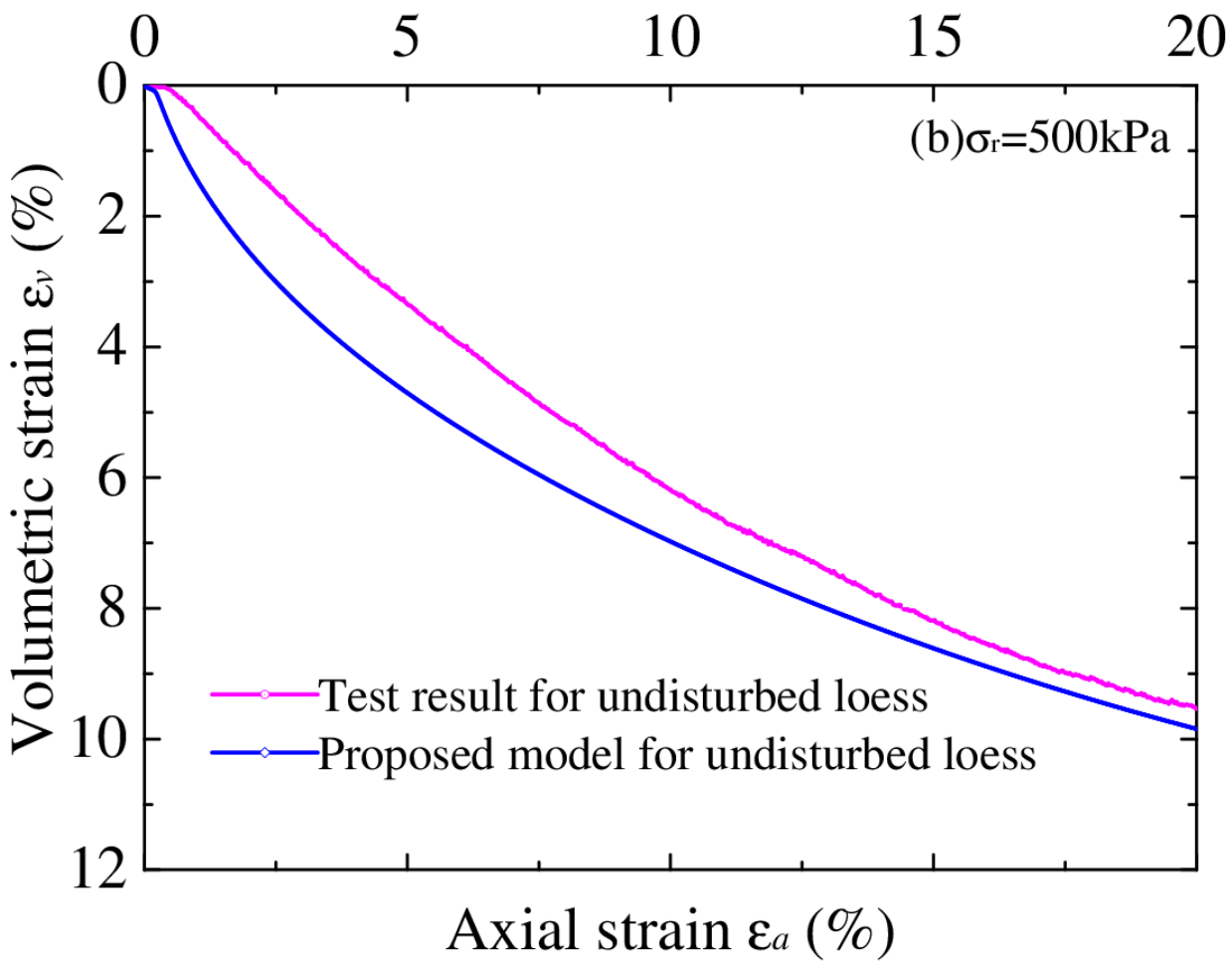

124

Fig. 12b

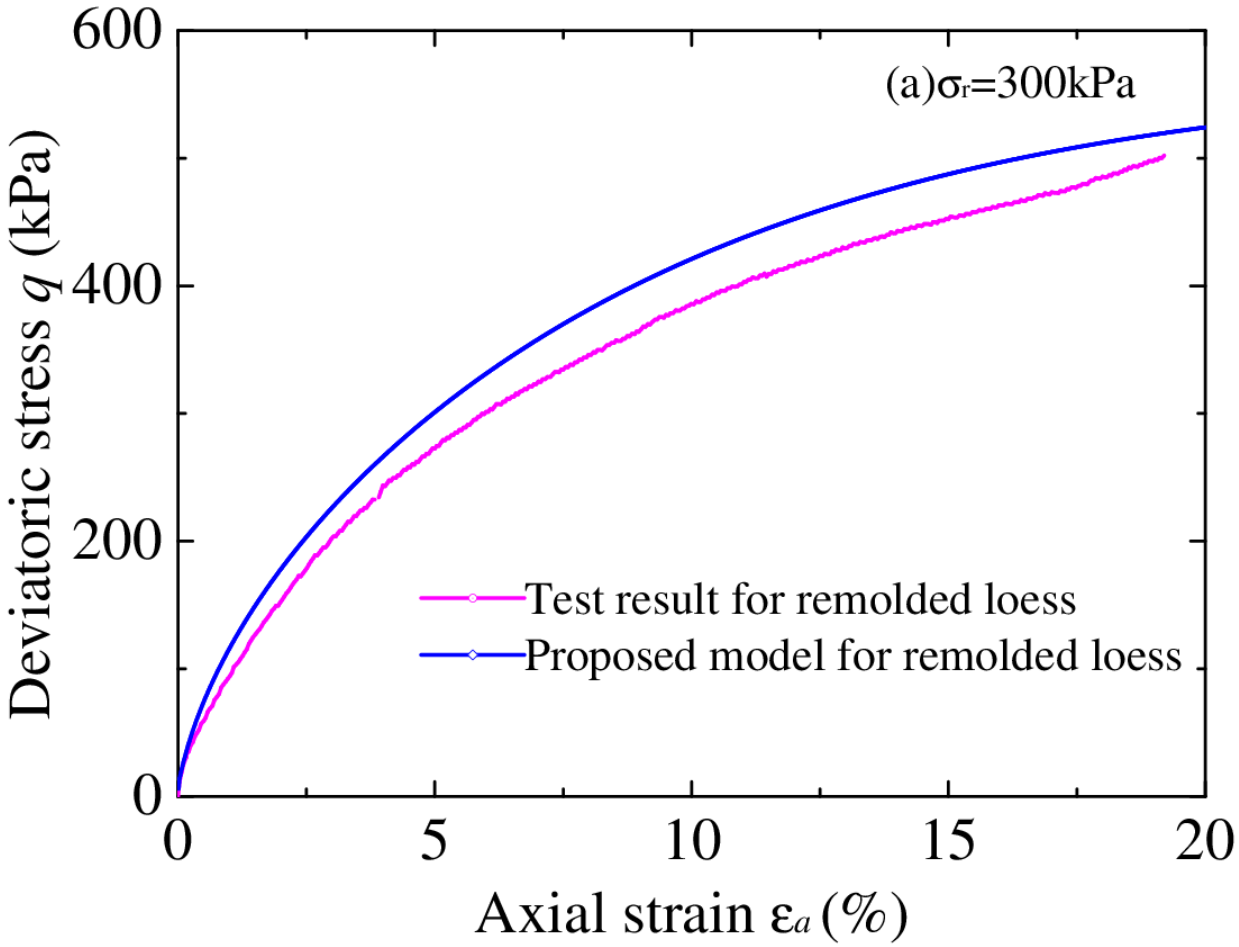

125

126

Fig. 13a

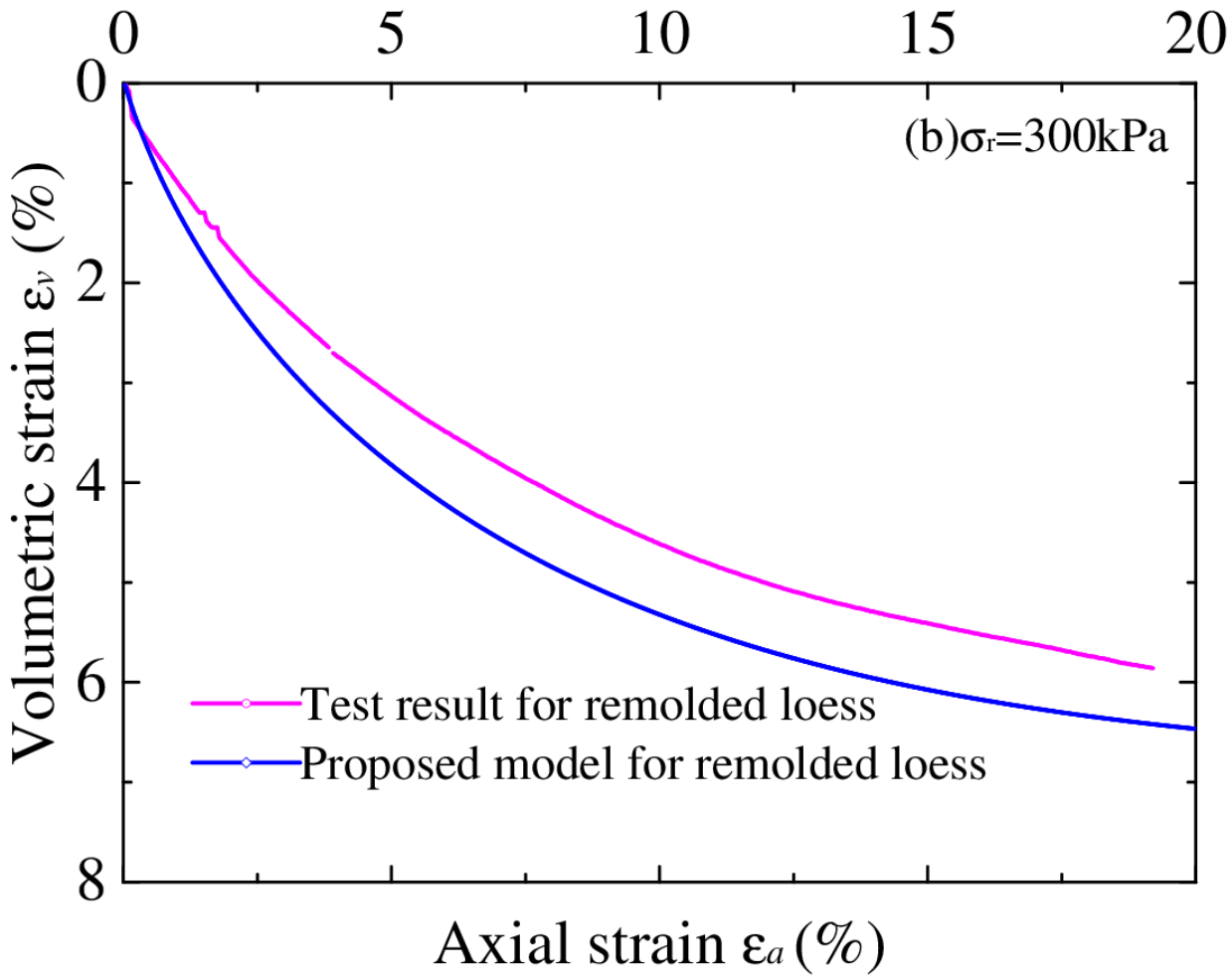
0
5
10
15
20
0
2
4
6
8
(b)σr=300kPa
Volumetric strain εv (%)
Test result for remolded loess
Proposed model for remolded loess
Axial strain εa (%)

Fig. 13b

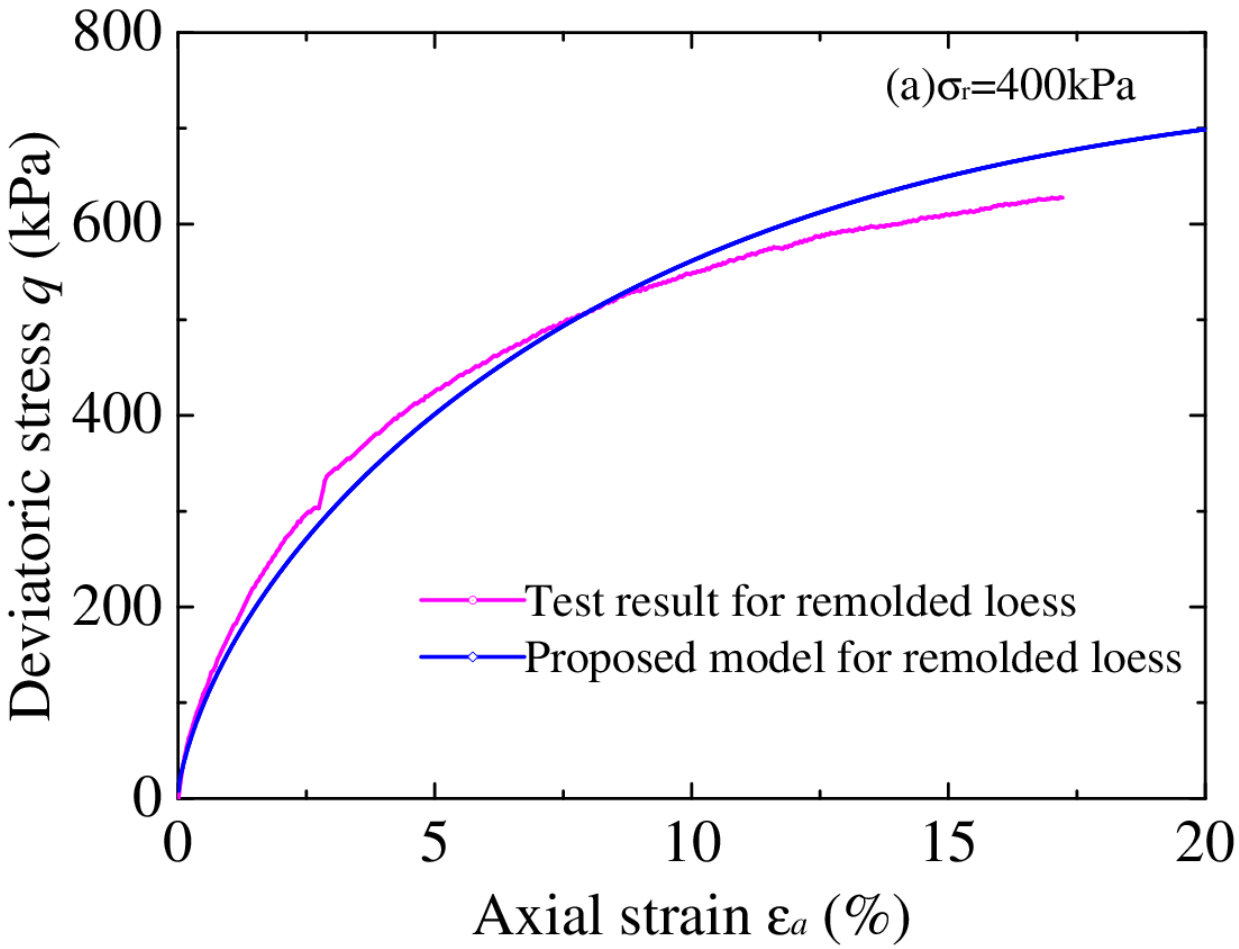
(a)σr=400kPa
Deviatoric stress q (kPa)
Axial strain εa (%)
Test result for remolded loess
Proposed model for remolded loess
0
200
400
600
800
0
5
10
15
20

Fig. 14a

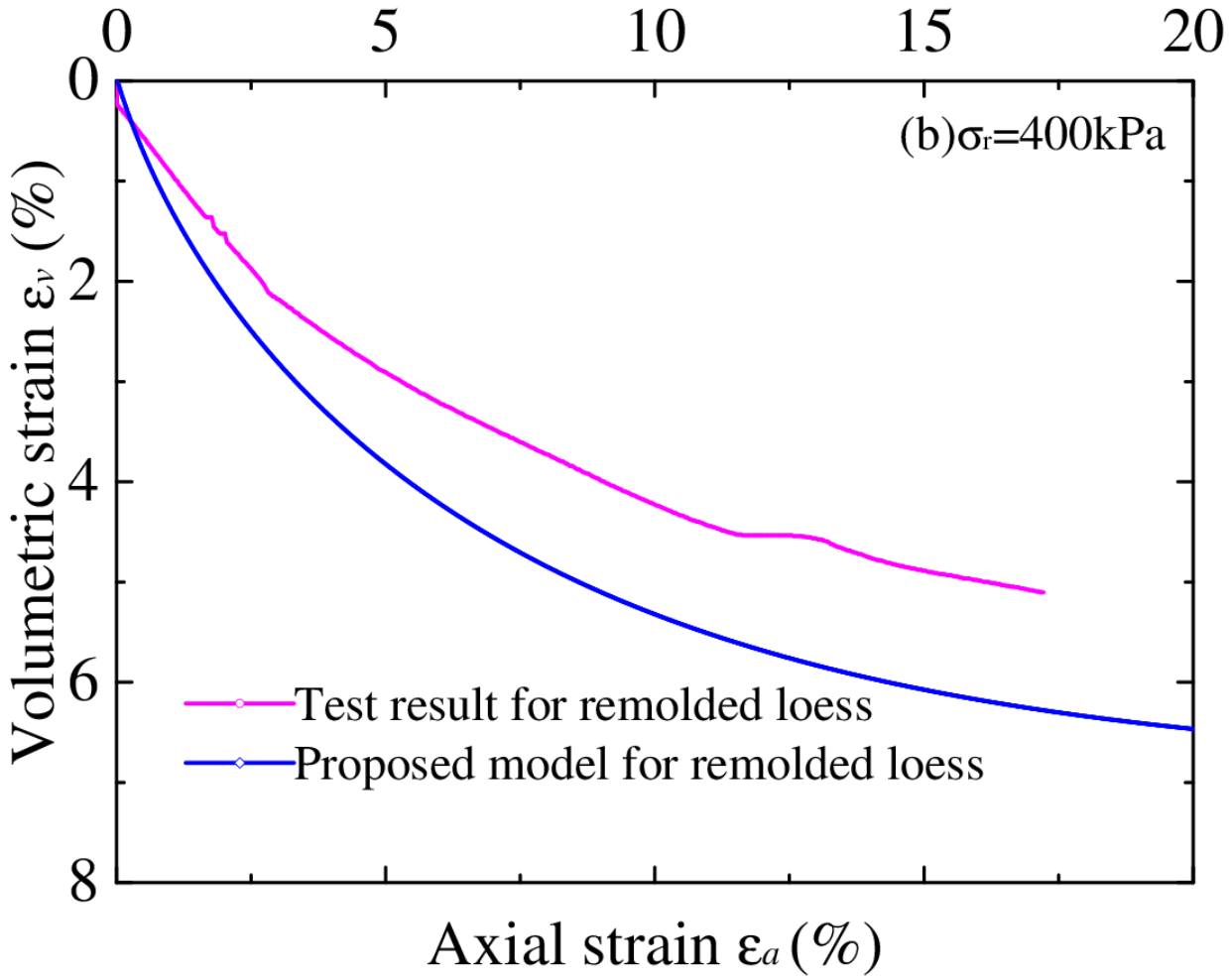
0
5
10
15
20
0
2
4
6
8
(b)σr=400kPa
Volumetric strain εv (%)
Test result for remolded loess
Proposed model for remolded loess
Axial strain εa (%)

Fig. 14b

133

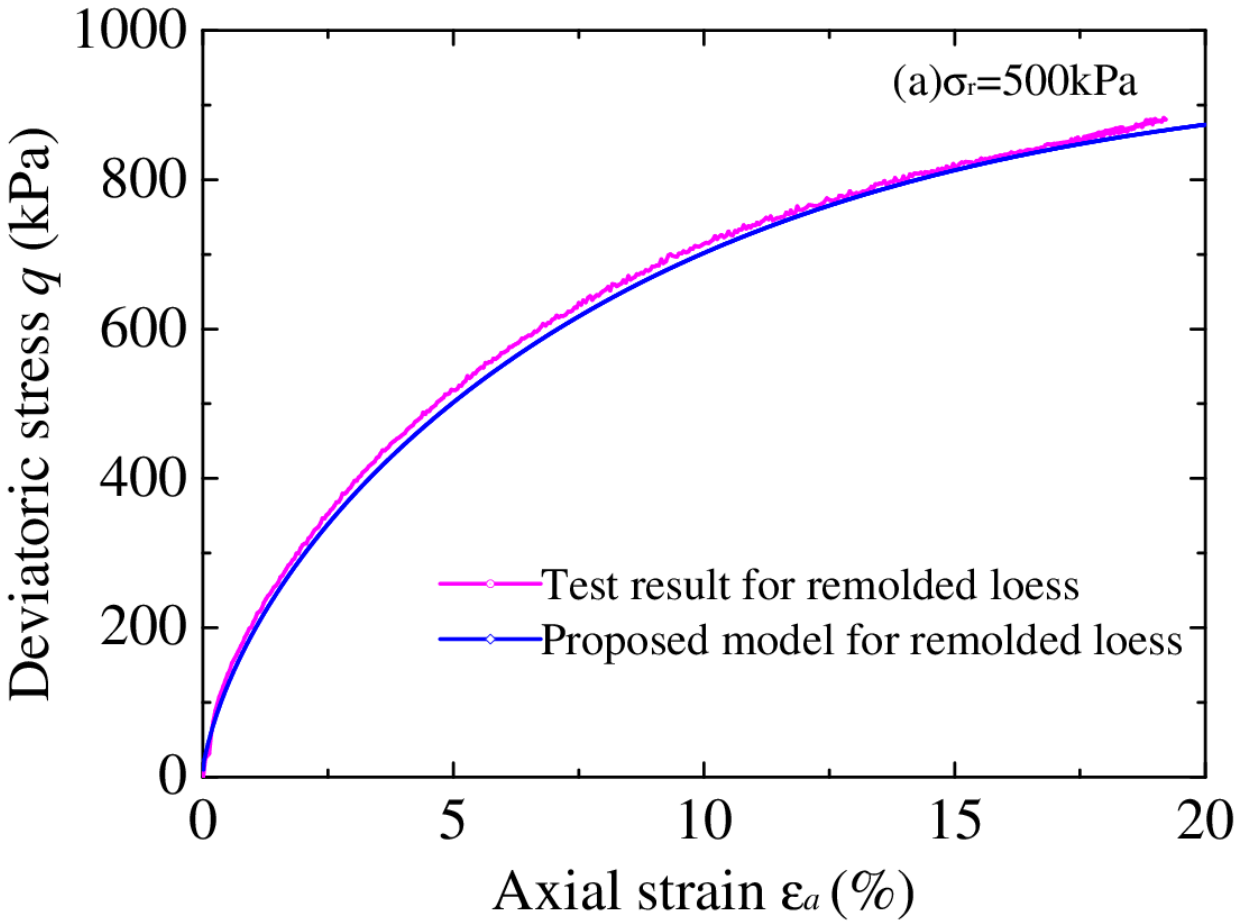

134

Fig. 15a

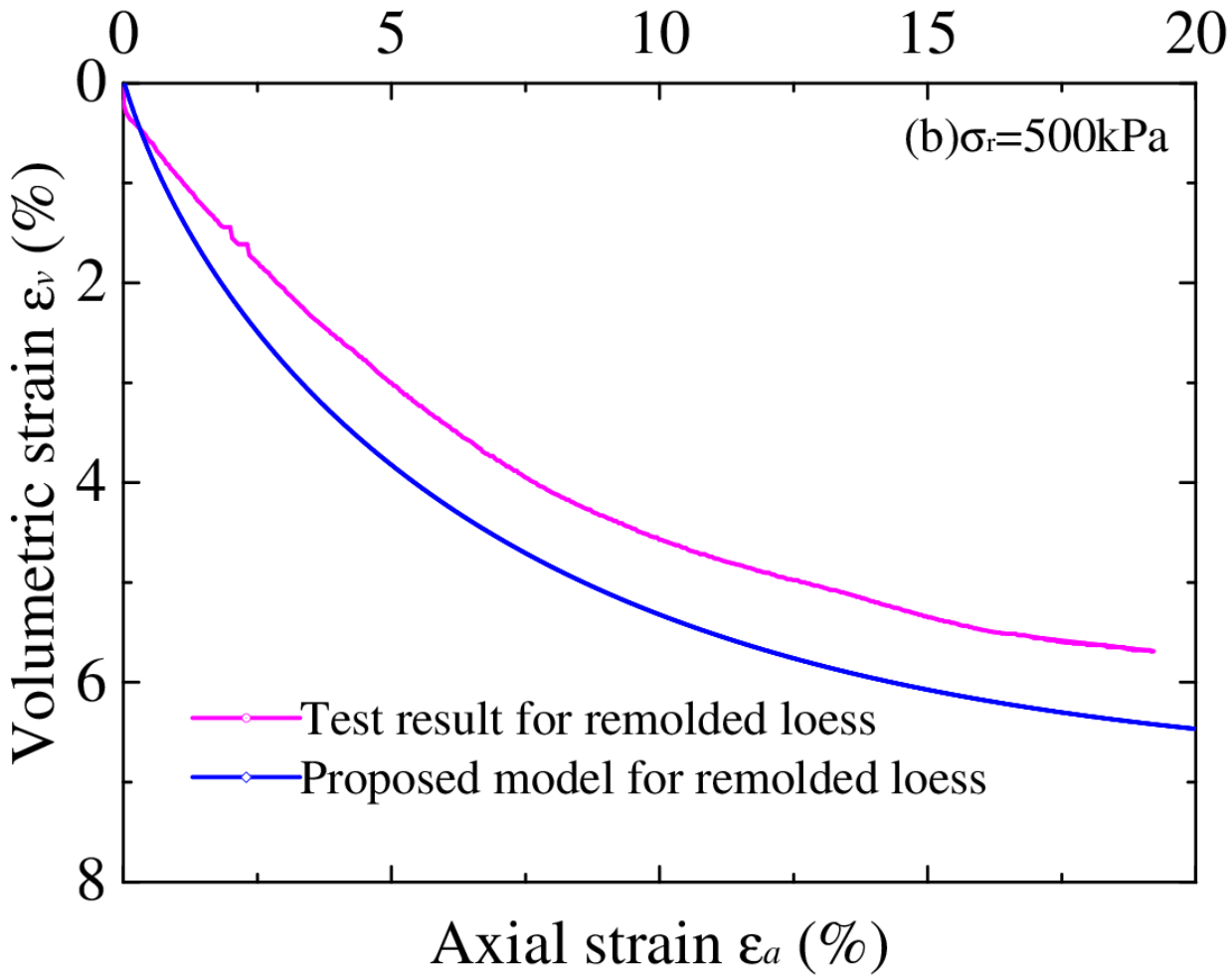

135

136

Fig. 15b

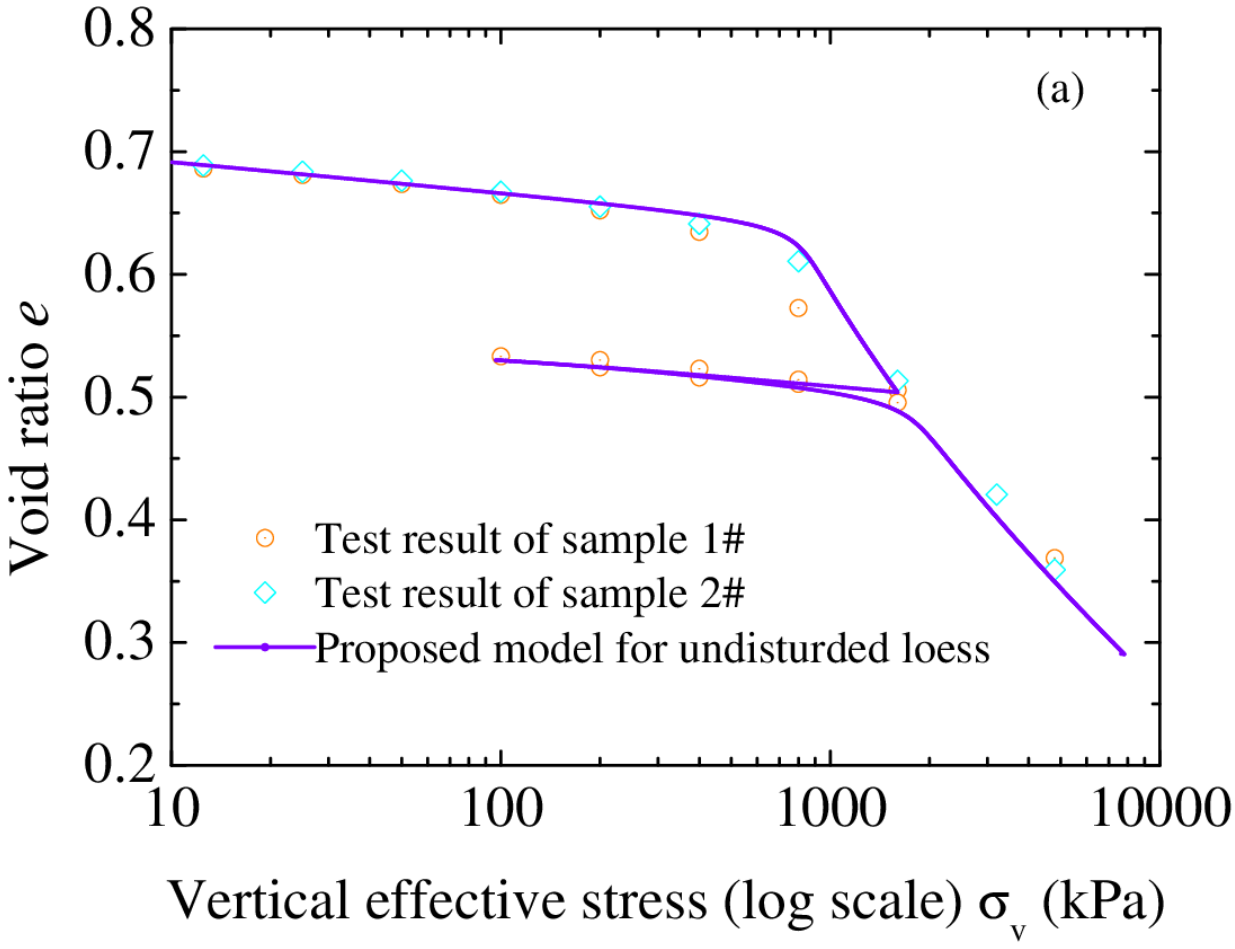
(a)
Void ratio e
0.8
0.7
0.6
0.5
0.4
0.3
0.2
10
100
1000
10000
Test result of sample 1#
Test result of sample 2#
Proposed model for undisturded loess
Vertical effective stress (log scale) σv (kPa)

Fig. 16a

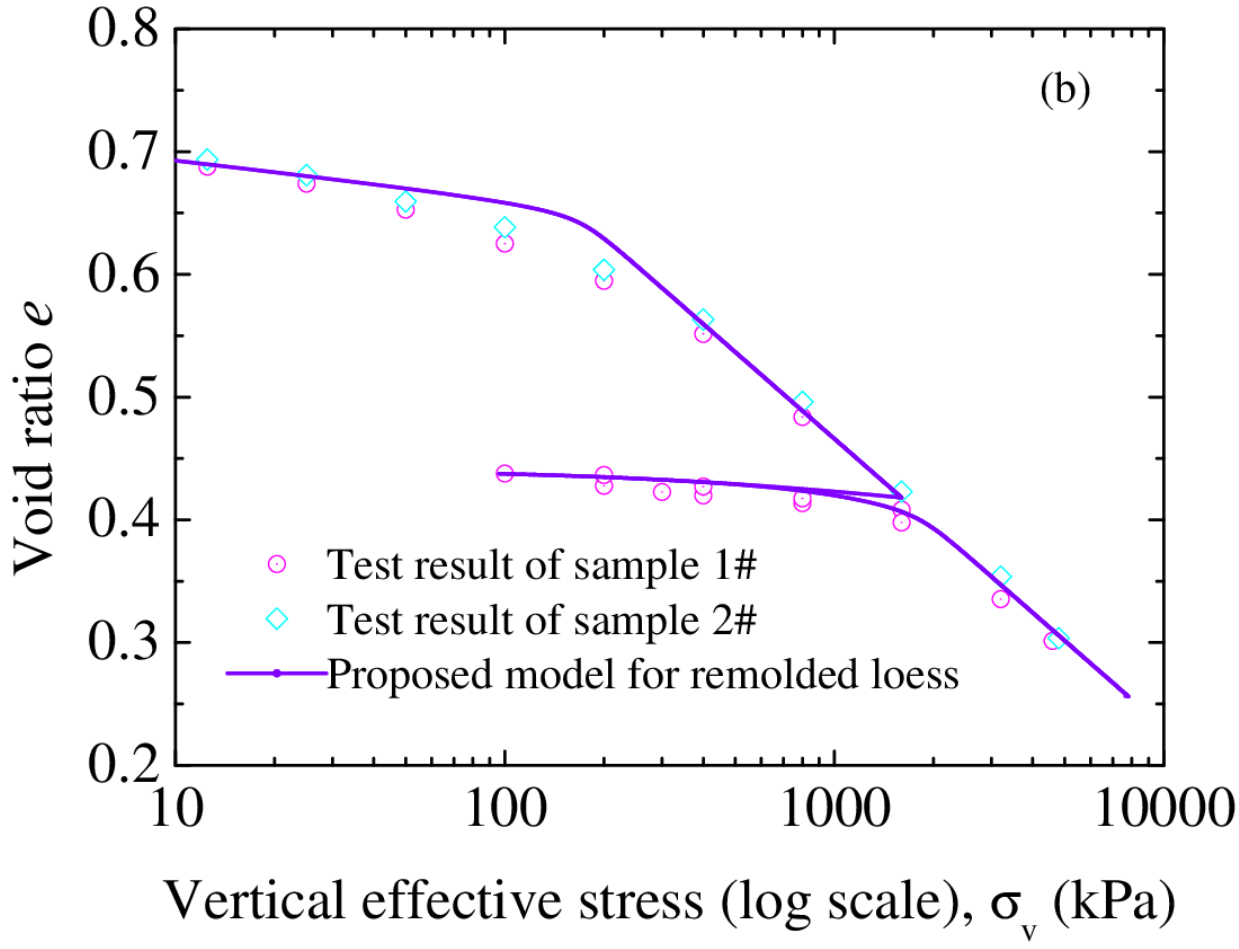
(b)
Void ratio e
0.8
0.7
0.6
0.5
0.4
0.3
0.2
10
100
1000
10000
Test result of sample 1#
Test result of sample 2#
Proposed model for remolded loess
Vertical effective stress (log scale), σv (kPa)

Fig. 16b